Jin M, **Sawa H**, Suzuki T, Shimizu K, Makino Y, Tanaka S, Nojima T, Fujioka Y, Asamoto M, Suko N, Nagashima K: Investigation of simian virus 40 large T antigen in 18 autopsied malignant mesothelioma patients in Japan. ***J Med Virol*** **74**: 668-676, 2004

Henmi C, **Sawa H**, Iwata H, Orba Y, Tanaka S, Nagashima K: Isolation of a monoclonal antibody recognizing a cell-surface molecule as a receptor for JC virus. ***Biochem Biophys Res Commun.*** **327**: 242-251, 2005

Henmi C, **Sawa H**, Iwata H, Orba Y, Tanaka S, Nagashima K. Establishment of an immunoscreening system using recombinant VP1 protein for the isolation of a monoclonal antibody that blocks JC virus infection. ***Biochem Biophys Res Commun*** 327: 242-251, 2005.

Suzuki T, Okada Y, Semba S, Orba Y, Yamanouchi S, Endo S, Tanaka S, Fujita T, Kuroda S, Nagashima K, **Sawa H**. Identification of FEZ1 as a Protein That Interacts with JC Virus Agnoprotein and Microtubules. ***J Biol Chem*** 280: 24948-24956, 2005.

Okada Y, Suzuki T, Sunden Y, Orba Y, Kose S, Imamoto N, Takahashi H, Tanaka S, Hall WW, Nagashima K, **Sawa H**. Dissociation of heterochromatin protein 1 from lamin B receptor induced by human polyomavirus agnoprotein: role in nuclear egress of viral particles. ***EMBO Rep*** 6: 452-457, 2005.

Ishida M, Tanaka S, Ohki M, **Ohta T.** BRM and BRG1 Negatively Regulate Transcriptional Activity of the Synovial Sarcoma Translocation Gene Product. ***Genes Cells*** **9**: 419-428, 2004.

仲　一仁、陳　晨、**本山　昇**. DNA ダメージチェックポイントとがん抑制メカニズム. ***実験医学*** **22**: 1793-1799, 2004.

III. 研究成果の刊行物・別刷

ELSEVIER

DNA damage tumor suppressor genes and genomic instability

Noboru Motoyama[1,*] and Kazuhito Naka[1,2]

Disruption of the mechanisms that regulate cell-cycle checkpoints, DNA repair, and apoptosis results in genomic instability and the development of cancer in multicellular organisms. The protein kinases ATM and ATR, as well as their downstream substrates Chk1 and Chk2, are central players in checkpoint activation in response to DNA damage. Histone H2AX, ATRIP, as well as the BRCT-motif-containing molecules 53BP1, MDC1, and BRCA1 function as molecular adapters or mediators in the recruitment of ATM or ATR and their targets to sites of DNA damage. The increased chromosomal instability and tumor susceptibility apparent in mutant mice deficient in both p53 and either histone H2AX or proteins that contribute to the nonhomologous end-joining mechanism of DNA repair indicate that DNA damage checkpoints play a pivotal role in tumor suppression.

Addresses
[1]Department of Geriatric Research, National Institute for Longevity Sciences, 36-3 Gengo, Morioka, Obu, Aichi 474-8522, Japan
[2]Department of Molecular Biology, Okayama University Graduate School of Medicine and Dentistry, 2-5-1 Shikata-cho, Okayama 700-8558, Japan
*e-mail: motoyama@nils.go.jp

Current Opinion in Genetics & Development 2004, **14**:11–16

This review comes from a themed issue on
Oncogenes and cell proliferation
Edited by Zena Werb and Gerard Evan

0959-437X/$ – see front matter

DOI 10.1016/j.gde.2003.12.003

Abbreviations

AT	ataxia telangiectasia
ATM	AT mutated
ATR	ATM- and Rad3-related
ATRIP	ATR-interacting protein
DNA-PK$_{cs}$	catalytic subunit of DNA-dependent protein kinase
IR	ionizing radiation
MDC1	mediator of DNA damage checkpoint protein 1
NBS	Nijmegen breakage syndrome
NHEJ	nonhomologous end joining
RPA	replication protein A
SMC	structural maintenance of chromosomes

Introduction

Environmental insults, including ultraviolet light, ionizing radiation (IR), and oxidative stress, such as that attributable to reactive oxygen species derived from oxidative metabolism, continually damage the genome of cells. In dividing cells, it is also prone to the introduction of errors during DNA replication and mitosis. Organisms have evolved mechanisms that maintain genomic integrity by inducing cell cycle arrest in response to DNA damage. Such checkpoint mechanisms allow the cell time to repair the DNA damage before cell cycle progression is resumed, or, if the damage is too extensive, they trigger apoptosis or cellular senescence. Defective checkpoint responses can thus result in genomic instability and lead to the transformation of normal cells into cancer cells. In familial cancer syndromes such as ataxia telangiectasia (AT), AT-like disorder, Li–Fraumeni syndrome, Nijmegen breakage syndrome (NBS), Fanconi anemia, and hereditary breast cancer, the mutated genes are involved in cell-cycle checkpoints or repair of DNA damage. Both ATM (AT mutated) and ATR (ATM- and Rad3-related) are members of the phosphatidylinositol 3-kinase–related kinase (PIKK) family of protein kinases and regulate a large number of proteins, including the kinases Chk1 and Chk2, that function in checkpoints activated during G_1, S, or G_2 phases of the cell cycle in response to DNA damage [1]. Here we review recent progress in the characterization of cell-cycle checkpoint mechanisms mediated by ATM, ATR, and their downstream targets Chk1 and Chk2 as well as insight gained into the roles of these mechanisms in DNA repair, the induction of apoptosis or senescence, and tumor suppression.

Sensing and signaling DNA damage

ATM and ATR trigger diverse cellular responses to DNA damage or stalled DNA replication during activation of the G_1–S, intra-S, or G_2 checkpoints [1]. ATM is encoded by the gene that is mutated in individuals with AT, which is characterized by progressive neurological degeneration, telangiectasia, growth retardation, specific immunodeficiency, a high sensitivity to IR, and an increased incidence of malignancy. A splicing mutation of the *ATR* gene has been identified in individuals with Seckel syndrome, an autosomal recessive disorder characterized by intrauterine growth retardation, dwarfism, microcephaly, and mental retardation [2]. Patients with Seckel syndrome are also at increased risk of developing myelodysplasia and acute myeloid leukemia, and a fibroblast cell line derived from an affected individual manifests a defective response to DNA damage.

Histone H2AX, 53BP1, BRCA1, MDC1, and NBS1 are all targets for ATM- or ATR-mediated phosphorylation and participate in transmission of the DNA damage signal to downstream molecules such as Chk1 and Chk2. The molecular mechanism of the sensing of DNA damage, however, remains elusive. Although phosphorylation of histone H2AX, yielding γ-H2AX, is dispensable for the

initial recognition of DNA damage [3], γ-H2AX is essential for the recruitment of 53BP1, BRCA1, MDC1, and the MRE11–RAD50–NBS1 complex to the site of DNA damage [3–5,6•,7•]. Cells from mice that lack the *H2AX* gene manifest a G_2 checkpoint defect similar to that apparent in ATM-deficient cells exposed to low doses (but not high doses) of IR [7•]; they also develop chromosomal instability after IR [4,5]. 53BP1 is an important mediator of DNA-damage signaling and is required for cell-cycle arrest in response to activation of the intra-S or G_2 checkpoint [7•–9•]. 53BP1 binds to p53, Chk2, and BRCA1, and it regulates the phosphorylation of Chk2, SMC1 (structural maintenance of chromosomes 1), and BRCA1 at sites of DNA strand breakage after exposure of cells to IR. 53BP1-deficient mice, like *ATM* knockout mice, are growth retarded, immune deficient, radiation sensitive, and cancer prone [10]. BRCA1 is necessary for activation of Chk1 during DNA damage–induced intra-S or G_2 arrest [11]. MDC1 (mediator of DNA damage checkpoint protein 1) is important in the formation of DNA damage induced foci containing 53BP1, BRCA1, and MRE11–RAD50–NBS1 [6•,12•]. Cells lacking MDC1 are sensitive to IR and fail to activate the intra-S and G_2 checkpoints [6•,12•,13•]. Hence, 53BP1, BRCA1, and MDC1 — all of which possess a BRCT (BRCA1 C-terminal) motif — appear to function as adaptor molecules that mediate the recruitment of ATM, ATR, and their targets to the sites of DNA damage.

A complex of ATR and ATRIP (ATR-interacting protein) phosphorylates and activates Chk1 in response to DNA replication stress or DNA damage. ATRIP also interacts with replication protein A (RPA) bound to single-stranded DNA at sites of DNA damage [14]. RPA thus recruits the ATRIP–ATR complex to damaged DNA and facilitates its recognition of phosphorylation targets such as RAD17 and RAD9 during initiation of checkpoint signaling. The PCNA-like complex RAD1–RAD9-Hus1 (also known as the 9-1-1 complex) and the RFC-like (Replication Factor C like) protein RAD17 are candidates for the DNA damage sensor. Hus1 acts upstream of Chk1 in the DNA-damage response [15]. The phosphorylation of RAD17 requires Hus1, suggesting that the 9-1-1 complex recruited by RAD17 facilitates substrate recognition by ATR [16].

Imaging of living human cells with damaged DNA has provided evidence of distinct spatiotemporal dynamics of Chk2 and NBS1 [17]. Whereas NBS1 is recruited immediately to the sites of DNA damage and undergoes dynamic exchange in close vicinity to such sites, activated Chk2 is rapidly redistributed throughout the surrounding region of the nucleus including undamaged areas. These observations indicate that Chk2 acts to spread the checkpoint signal, resulting in the activation of downstream targets, such as p53 and CDC25A, in a larger region of the nucleus.

The G_1–S checkpoint: role of an ATM–Chk2–p53 pathway

The most fundamental event in the G_1–S checkpoint is the stabilization and activation of p53, which, in turn, induces transcription of the gene for p21, an inhibitor of the cyclin E–CDK2 complex. Signals that regulate p53 ultimately converge to disrupt the interaction between p53 and its negative regulator MDM2. The MDM2 oncoprotein is a RING-finger-type ubiquitin ligase that ubiquitinates both itself and p53; its binding to the N-terminus of p53 thus results in the ubiquitination of p53 and its consequent degradation by the 26S proteasome. ATM is implicated in p53 regulation by the observation that it directly phosphorylates p53 on Ser-15, which abrogates the p53–MDM2 interaction and allows p53 to accumulate. ATM also phosphorylates MDM2 on Ser-395, which interferes with the nuclear export of the MDM2–p53 complex. Furthermore, ATM phosphorylates the tyrosine kinase c-ABL on Ser-465, and the activated c-ABL in turn contributes to p53 stabilization by phosphorylating MDM2 on Tyr-394 [18].

ATM phosphorylates Chk2 on Thr-68 and thereby promotes the oligomerization of Chk2 by creating a specific binding site for the FHA domain of another Chk2 molecule [19,20]. The homodimerization of Chk2 also facilitates *trans*-phosphorylation of the C-terminal kinase domain (Thr-383, Thr-387), which is required for full activation of Chk2. Human Chk2 functions in G_1 arrest in response to IR through p53. Cells derived from Chk2-deficient mice thus have a defective G_1–S checkpoint [21••,22••]. Although Chk2 forms a stable complex with p53 [23] and has been proposed to activate p53 by phosphorylating it — Ser-20 in human, Ser-23 in mouse — both the stabilization and Ser-23 phosphorylation of p53 are evident in Chk2-deficient mouse cells after exposure to IR [21••,22••]. The transcriptional induction of p53 target genes, such as those for p21, Bax, and Noxa, is impaired, but, in Chk2-deficient cells, consistent with the observation that Chk2 is rate-limiting for p53 *trans*-activation activity in U2OS human cancer cells [17] and indicating that Chk2 is essential for p53 activation in response to DNA damage *in vivo* [21••,22••].

The intra-S checkpoint: role of ATM-mediated pathways

Radio-resistant DNA synthesis is a phenotypic hallmark of cells derived from individuals with AT, AT-like disorder, Fanconi anemia, or NBS, indicating that the proteins encoded by the genes that are mutated in these various disorders play a role in the intra–S phase checkpoint. Two pathways that have been implicated in activation of the intra-S checkpoint are those mediated by ATM–Chk2–CDC25A and by ATM–NBS1–SMC1 [24].

CDC25A is a phosphatase that activates CDK2 by dephosphorylation at Thr-14 and Tyr-15, which is required for

DNA synthesis. Chk2 that has been activated by ATM phosphorylates CDC25A on Ser-123, resulting in its degradation by the ubiquitin-proteasome pathway and delay of S-phase progression. The observation that human cells expressing functionally impaired Chk2 mutants manifest radio-resistant DNA synthesis indicates that Chk2 plays a role in the intra-S checkpoint. Defects in this checkpoint are not apparent, however, in cells from Chk2-deficient mice, possibly because loss of Chk2 is functionally compensated for by other molecules such as Chk1 [21••,22••]. Indeed, Chk1 activated by ATM or ATR also phosphorylates CDC25A and is implicated in the intra-S checkpoint [25,26].

The MRE11–RAD50–NBS1 complex is required for normal function of the intra-S checkpoint. ATM phosphorylates NBS1 on Ser-343 and thereby activates the intra-S checkpoint. Both SMC1 and SMC3 contain coiled-coil domains and are components of the cohesin complex that is required for the cohesin of sister chromatids. SMC1 is phosphorylated on Ser-957 and Ser-966 by ATM in an NBS1-dependent manner in response to exposure of cells to IR, and this phosphorylation of SMC1 is required for activation of the intra-S checkpoint [27,28]. The intra-S checkpoint is thus regulated by two parallel pathways mediated by ATM–NBS1–SMC1 and ATM/ATR–Chk1/Chk2–CDC25A [24]. The mediator–adaptor proteins 53BP1, BRCA1, and MDC1 also contribute to the intra-S checkpoint by regulating the phosphorylation of downstream proteins such as Chk1, Chk2, and NBS1, although their precise mechanisms of action remain unclear.

The G_2 checkpoint: roles of ATM and ATR

The central event in activation of the G_2 checkpoint is inhibition of the mitosis-promoting phosphatase CDC25C. Studies of (embryonic) cells deficient in ATM, ATR, or Chk1 have shown that the ATM/ATR–Chk1 pathway is responsible for activation of the G_2 checkpoint in response to DNA damage induced by IR [29•]. ATR and ATM each activate Chk1 by phosphorylation on Ser-317 and Ser-345, and activated Chk1 phosphorylates CDC25C on Ser-217 and thereby creates a binding site for 14-3-3 protein. Its interaction with 14-3-3 prevents CDC25C from dephosphorylating and activating the mitotic kinase complex cyclin B–Cdc2, thus effectively blocking cells with damaged DNA from entering mitosis. Although ATR and ATM each contribute to an early delay in entry into M phase, ATR is mostly responsible for a later phase of G_2 arrest [29•]. Although Chk2 has been thought to contribute to DNA damage–induced G_2 arrest, activation of the G_2 checkpoint in response to IR is intact in Chk2-deficient cells, even at low doses of IR [7•].

In contrast to G_2 arrest induced by DNA damage, ATR deficiency does not affect the DNA replication (S–M) checkpoint [29•]. Neither Chk1 phosphorylation nor inhibitory phosphorylation of Cdc2 on Thr-14 and Tyr-15 occurs in response to stalled DNA replication in ATR-deficient cells, suggesting that the replication checkpoint in mammalian somatic cells is independent of ATR–Chk1 and inhibitory phosphorylation of Cdc2.

Apoptosis induction and tumor suppression

Cells that experience a level of DNA damage beyond repair either enter senescence or undergo apoptosis to prevent the propagation of carcinogenic genetic alterations. The p53 tumor suppressor protein plays a central role in the decision of a cell to undergo apoptosis after exposure to diverse stresses, including DNA damage. As described above, Chk2 is an important regulator of both the stability and the *trans*-activation activity of p53 in cells exposed to IR [21••,22••]. Activation of Chk2 that leads to p53-mediated apoptosis is regulated by both ATM-dependent and ATM-independent pathways, the latter of which might be mediated by the newly identified ATX [1]. The activation of p53 in response to DNA damage results in the induction of p53 target genes — such as those for Noxa, Bax, and Puma — that contribute to apoptosis. The induction of these proapoptotic genes by p53 also appears to be triggered by phosphorylation of p53 on Ser-46 by HIPK2 (homeodomain-interacting protein kinase 2), a nuclear serine–threonine kinase that is localized to subnuclear structures known as PML oncogenic domains (PODs) [30,31]. Recent studies indicate that p53 itself translocates to mitochondria to induce apoptosis [32,33]. The precise mechanism by which Chk2 regulates the apoptosis-inducing activity of p53, however, remains unclear. Chk2 also regulates the activity of the transcription factor E2F1 by phosphorylation of Ser-364 in response to DNA damage, again resulting in the induction of apoptosis [34]. The phosphorylation of PML on Ser-117 by Chk2 also occurs during the induction of p53-independent apoptosis [35].

Cooperation of cell-cycle checkpoints and DNA repair in tumor suppression

Mice that lack either ATM or 53BP1 [10], both of which are upstream mediators of the DNA-damage response and participate in both cell-cycle checkpoint and DNA-repair pathways, are predisposed to the development of cancer. The contributions of defective DNA repair and impaired checkpoint function to tumor development have been investigated with mice that are deficient in both p53 and proteins important in the nonhomologous end joining (NHEJ) pathway of DNA repair, such as Xrcc4, DNA ligase IV, DNA-PK_{cs} (catalytic subunit of DNA-dependent protein kinase), and Ku80. Although the lack of p53 rescues the embryonic lethality phenotype of Xrcc4- or ligase-IV-deficient mice, Xrcc4–p53 and ligase-IV–p53 double mutants, as well as DNA-PK_{cs}–p53 and Ku80–p53 double-knockout mice, succumb to pro-B cell lymphoma between 6 and 16 weeks after birth

[36••,37••]. These various mice manifest oncogenic gene amplification in what has been termed a complicon. Mice lacking both H2AX and p53 also rapidly develop immature T and B lymphomas as well as solid tumors [38••,39••]. DNA-PK$_{cs}$, Ku80, or H2AX single-knockout mice survive without an increased susceptibility to cancer. The increased chromosomal instability in the double-knockout mice that are defective in both NHEJ and cell-cycle checkpoint function thus indicates that checkpoint responses play an important role in the maintenance of genomic integrity that is not a result of direct participation in DNA repair.

Mutations in the mismatch repair genes *MLH1* or *MSH2* result in microsatellite instability and hereditary nonpolyposis colon cancer (HNPCC). Cells deficient in mismatch repair proteins also show defects in intra-S and G_2 checkpoints [40,41]. ATM- or ATR-dependent phosphorylation and activation of Chk1 or Chk2 and subsequent degradation of the downstream target CDC25A are thus abrogated in such cells [40,41]. MSH2 binds to Chk2 and MLH1 associates with ATM, and the presence of the mismatch repair complex at sites of DNA damage is required for the phosphorylation and activation of Chk2 by ATM. Networking between DNA repair and checkpoint molecules is thus important for maintenance of genomic integrity and tumor suppression.

Figure 1

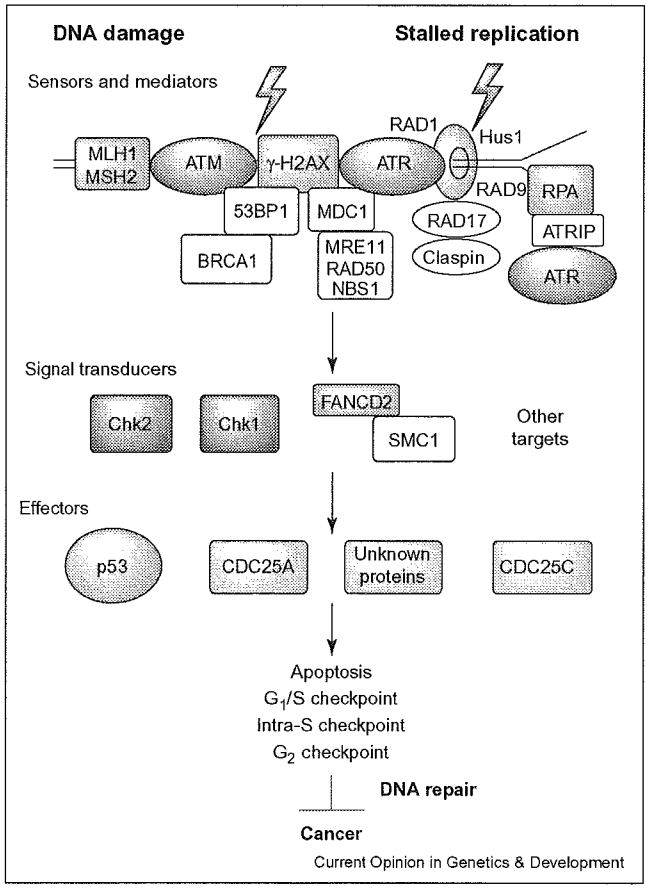

DNA damage checkpoint machinery. In response to DNA damage, ATM and ATR phosphorylate histone H2AX and thereby facilitate the recruitment and phosphorylation of mediators such as MDC1, 53BP1, BRCA1, and the MRE11–RAD50–NBS1 complex. Stalling of the DNA replication fork results in the recruitment of the ATR–ATRIP complex by RPA. In turn, the formation of nuclear foci of mediator complexes promotes transmission of the DNA damage signal to downstream targets such as Chk1, Chk2, FANCD2, and SMC1. The PCNA-like RAD1–RAD9–Hus1 complex, the RFC-like RAD17, and Claspin may collaborate in checkpoint regulation by detecting different aspects of a DNA replication fork. The mismatch repair proteins MLH1 and MSH also implicate in the activation of ATM-Chk2 pathway. The kinases Chk1 and Chk2 phosphorylate effectors such as p53, CDC25A, and CDC25C and thereby delay cell cycle progression or induce senescence or apoptosis via activation of the G_1–S, intra-S, or G_2 cell cycle checkpoints. Thus, these DNA damage checkpoint mechanisms cooperate with DNA repair machinery to suppress genomic instability and cancer.

Conclusions

We have provided an overview of recent advances in the characterization of cell-cycle checkpoints and their roles in facilitation of the repair of DNA damage and tumor suppression (Figure 1). The increased genomic instability apparent in cancer cells reflects the fact that the accumulation of genetic mutations as a result of defects in cell-cycle checkpoints or DNA repair activity is an important cause of tumorigenesis. Given that mutations in the genes for various proteins that contribute to checkpoint function or DNA repair are responsible for hereditary cancer syndromes as well as sporadic tumors, the activation of cell-cycle checkpoints in response to DNA damage is essential for maintenance of genomic integrity and tumor suppression.

Acknowledgements

We thank Hiroyuki Takai and members of our laboratory for stimulating discussions. Research in the authors' laboratory was supported by Grant-in-Aid for Scientific Research from The Ministry of Education, Culture, Sports, Science and Technology of Japan.

References and recommended reading

Papers of particular interest, published within the annual period of review, have been highlighted as:

- • of special interest
- •• of outstanding interest

1. Shiloh Y: **ATM and related protein kinases: safeguarding genome integrity**. *Nat Rev Cancer* 2003, **3**:155-168.

2. O'Driscoll M, Ruiz-Perez VL, Woods CG, Jeggo PA, Goodship JA: **A splicing mutation affecting expression of ataxia-telangiectasia and Rad3-related protein (ATR) results in Seckel syndrome**. *Nat Genet* 2003, **33**:497-501.

3. Celeste A, Fernandez-Capetillo O, Kruhlak MJ, Pilch DR, Staudt DW, Lee A, Bonner RF, Bonner WM, Nussenzweig A: **Histone H2AX phosphorylation is dispensable for the initial recognition of DNA breaks**. *Nat Cell Biol* 2003, **5**:675-679.

4. Bassing CH, Chua KF, Sekiguchi J, Suh H, Whitlow SR, Fleming JC, Monroe BC, Ciccone DN, Yan C, Vlasakova K *et al.*: **Increased ionizing radiation sensitivity and genomic instability in the absence of histone H2AX**. *Proc Natl Acad Sci USA* 2002, **99**:8173-8178.

5. Celeste A, Petersen S, Romanienko PJ, Fernandez-Capetillo O, Chen HT, Sedelnikova OA, Reina-San-Martin B, Coppola V, Meffre E, Difilippantonio MJ *et al.*: **Genomic instability in mice lacking histone H2AX**. *Science* 2002, **296**:922-927.

6. • Stewart GS, Wang B, Bignell CR, Taylor AM, Elledge SJ: **MDC1 is a mediator of the mammalian DNA damage checkpoint**. *Nature* 2003, **421**:961-966.
See annotation [13•].

7. • Fernandez-Capetillo O, Chen HT, Celeste A, Ward I, Romanienko PJ, Morales JC, Naka K, Xia Z, Camerini-Otero RD, Motoyama N *et al.*: **DNA damage-induced G2-M checkpoint activation by histone H2AX and 53BP1**. *Nat Cell Biol* 2002, **4**:993-997.
See annotation [9•].

8. • DiTullio RA Jr, Mochan TA, Venere M, Bartkova J, Sehested M, Bartek J, Halazonetis TD: **53BP1 functions in an ATM-dependent checkpoint pathway that is constitutively activated in human cancer**. *Nat Cell Biol* 2002, **4**:998-1002.
See annotation [9•].

9. • Wang B, Matsuoka S, Carpenter PB, Elledge SJ: **53BP1, a mediator of the DNA damage checkpoint**. *Science* 2002, **298**:1435-1438.
References [7•–9•] show that 53BP1 using small interfering RNA-mediated depletion of 53BP1 or 53BP1-deficient cells that 53BP1 plays an important role for recruitment and phosphorylation of checkpoint proteins such as BRCA1 by ATM or ATR and that 53BP1 plays a central role in activation of both the intra-S and G_2 checkpoint in response to low dose (but not high dose) of IR. Thus, 53BP1 is either a critical adaptor or a mediator protein for DNA-damage signaling.

10. Ward IM, Minn K, van Deursen J, Chen J: **p53 binding protein 53BP1 is required for DNA damage responses and tumor suppression in mice**. *Mol Cell Biol* 2003, **23**:2556-2563.

11. Yarden RI, Pardo-Reoyo S, Sgagias M, Cowan KH, Brody LC: **BRCA1 regulates the G2/M checkpoint by activating Chk1 kinase upon DNA damage**. *Nat Genet* 2002, **30**:285-289.

12. • Goldberg M, Stucki M, Falck J, D'Amours D, Rahman D, Pappin D, Bartek J, Jackson SP: **MDC1 is required for the intra-S-phase DNA damage checkpoint**. *Nature* 2003, **421**:952-956.
See annotation [13•].

13. • Lou Z, Minter-Dykhouse K, Wu X, Chen J: **MDC1 is coupled to activated CHK2 in mammalian DNA damage response pathways**. *Nature* 2003, **421**:957-961.
References [6•,12•,13•] show that the BRCT-motif-containing protein MDC1 is phosphorylated in an ATM-dependent manner and rapidly localizes to sites of DNA damage in response to IR. Using small interfering RNA-mediated depletion of MDC1, they show that MDC facilitates the recruitment of checkpoint and DNA repair proteins such as BRCA1, thereby contributing to activation of the intra-S checkpoint. Thus MDC1 functions as either an adaptor or mediator protein for transducing signals from DNA damage.

14. Zou L, Elledge SJ: **Sensing DNA damage through ATRIP recognition of RPA-ssDNA complexes**. *Science* 2003, **300**:1542-1548.

15. Weiss RS, Leder P, Vaziri C: **Critical role for mouse Hus1 in an S-phase DNA damage cell cycle checkpoint**. *Mol Cell Biol* 2003, **23**:791-803.

16. Zou L, Cortez D, Elledge SJ: **Regulation of ATR substrate selection by Rad17-dependent loading of Rad9 complexes onto chromatin**. *Genes Dev* 2002, **16**:198-208.

17. Lukas C, Falck J, Bartkova J, Bartek J, Lukas J: **Distinct spatiotemporal dynamics of mammalian checkpoint regulators induced by DNA damage**. *Nat Cell Biol* 2003, **5**:255-260.

18. Goldberg Z, Vogt Sionov R, Berger M, Zwang Y, Perets R, Van Etten RA, Oren M, Taya Y, Haupt Y: **Tyrosine phosphorylation of Mdm2 by c-Abl: implications for p53 regulation**. *EMBO J* 2002, **21**:3715-3727.

19. Xu X, Tsvetkov LM, Stern DF: **Chk2 activation and phosphorylation-dependent oligomerization**. *Mol Cell Biol* 2002, **22**:4419-4432.

20. Ahn JY, Li X, Davis HL, Canman CE: **Phosphorylation of threonine 68 promotes oligomerization and autophosphorylation of the Chk2 protein kinase via the forkhead-associated domain**. *J Biol Chem* 2002, **277**:19389-19395.

21. •• Hirao A, Cheung A, Duncan G, Girard PM, Elia AJ, Wakeham A, Okada H, Sarkissian T, Wong JA, Sakai T *et al.*: **Chk2 is a tumor suppressor that regulates apoptosis in both an ataxia telangiectasia mutated (ATM)-dependent and an ATM-independent manner**. *Mol Cell Biol* 2002, **22**:6521-6532.
See annotation [22••].

22. •• Takai H, Naka K, Okada Y, Watanabe M, Harada N, Saito S, Anderson CW, Appella E, Nakanishi M, Suzuki H *et al.*: **Chk2-deficient mice exhibit radioresistance and defective p53-mediated transcription**. *EMBO J* 2002, **21**:5195-5205.
References [21••,22••] show that Chk2 is essential for IR-induced, p53-mediated apoptosis and regulates both the *trans*-activation activity and stability of p53 in response to IR.

23. Falck J, Lukas C, Protopopova M, Lukas J, Selivanova G, Bartek J: **Functional impact of concomitant versus alternative defects in the Chk2-p53 tumour suppressor pathway**. *Oncogene* 2001, **20**:5503-5510.

24. Falck J, Petrini JH, Williams BR, Lukas J, Bartek J: **The DNA damage-dependent intra-S phase checkpoint is regulated by parallel pathways**. *Nat Genet* 2002, **30**:290-294.

25. Zhao H, Watkins JL, Piwnica-Worms H: **Disruption of the checkpoint kinase 1/cell division cycle 25A pathway abrogates ionizing radiation-induced S and G2 checkpoints**. *Proc Natl Acad Sci USA* 2002, **99**:14795-14800.

26. Sorensen CS, Syljuasen RG, Falck J, Schroeder T, Ronnstrand L, Khanna KK, Zhou BB, Bartek J, Lukas J: **Chk1 regulates the S phase checkpoint by coupling the physiological turnover and ionizing radiation-induced accelerated proteolysis of Cdc25A**. *Cancer Cell* 2003, **3**:247-258.

27. Yazdi PT, Wang Y, Zhao S, Patel N, Lee EY, Qin J: **SMC1 is a downstream effector in the ATM/NBS1 branch of the human S-phase checkpoint**. *Genes Dev* 2002, **16**:571-582.

28. Kim ST, Xu B, Kastan MB: **Involvement of the cohesin protein, Smc1, in Atm-dependent and independent responses to DNA damage**. *Genes Dev* 2002, **16**:560-570.

29. • Brown EJ, Baltimore D: **Essential and dispensable roles of ATR in cell cycle arrest and genome maintenance**. *Genes Dev* 2003, **17**:615-628.
This paper shows that ATM and ATR regulate the G_2 checkpoint in response to IR, but that ATR is mostly responsible for maintenance of G_2 arrest. Checkpoint activation by either stalled or incomplete DNA replication does not depend on an ATR–Chk1 pathway in mammalian cells.

30. D'Orazi G, Cecchinelli B, Bruno T, Manni I, Higashimoto Y, Saito S, Gostissa M, Coen S, Marchetti A, Del Sal G *et al.*: **Homeodomain-interacting protein kinase-2 phosphorylates p53 at Ser 46 and mediates apoptosis**. *Nat Cell Biol* 2002, **4**:11-19.

31. Hofmann TG, Moller A, Sirma H, Zentgraf H, Taya Y, Droge W, Will H, Schmitz ML: **Regulation of p53 activity by its interaction with homeodomain-interacting protein kinase-2**. *Nat Cell Biol* 2002, **4**:1-10.

32. Mihara M, Erster S, Zaika A, Petrenko O, Chittenden T, Pancoska P, Moll UM: **p53 has a direct apoptogenic role at the mitochondria**. *Mol Cell* 2003, **11**:577-590.

33. Dumont P, Leu JI, Della Pietra AC III, George DL, Murphy M: **The codon 72 polymorphic variants of p53 have markedly different apoptotic potential**. *Nat Genet* 2003, **33**:357-365.

34. Stevens C, Smith L, La Thangue NB: **Chk2 activates E2F-1 in response to DNA damage**. *Nat Cell Biol* 2003, **5**:401-409.

35. Yang S, Kuo C, Bisi JE, Kim MK: **PML-dependent apoptosis after DNA damage is regulated by the checkpoint kinase hCds1/Chk2**. *Nat Cell Biol* 2002, **4**:865-870.

36. •• Difilippantonio MJ, Petersen S, Chen HT, Johnson R, Jasin M, Kanaar R, Ried T, Nussenzweig A: **Evidence for replicative repair of DNA double-strand breaks leading to oncogenic translocation and gene amplification**. *J Exp Med* 2002, **196**:469-480.
See annotation [37••].

37. •• Zhu C, Mills KD, Ferguson DO, Lee C, Manis J, Fleming J, Gao Y, Morton CC, Alt FW: **Unrepaired DNA breaks in p53-deficient cells lead to oncogenic gene amplification subsequent to translocations**. *Cell* 2002, **109**:811-821.
References [36••,37••] show that, although NHEJ-deficient mice exhibit a moderately increased susceptibility to cancer, combined deficiency of NHEJ and p53 results in the early development of pro-B lymphoma, suggesting that activation of the G_1–S checkpoint to allow DNA repair or apoptosis is important for tumor suppression.

38. •• Bassing CH, Suh H, Ferguson DO, Chua KF, Manis J, Eckersdorff M, Gleason M, Bronson R, Lee C, Alt FW: **Histone H2AX: a dosage-dependent suppressor of oncogenic translocations and tumors**. *Cell* 2003, **114**:359-370.
See annotation [39••].

39. •• Celeste A, Difilippantonio S, Difilippantonio MJ, Fernandez-Capetillo O, Pilch DR, Sedelnikova OA, Eckhaus M, Ried T, Bonner WM, Nussenzweig A: **H2AX haploinsufficiency modifies genomic stability and tumor susceptibility**. *Cell* 2003, **114**:371-383.
References [38••,39••] show that H2AX haploinsufficiency causes genomic instability in either normal or p53-deficient cells and increases susceptibility to cancer in the absence of p53, indicating that H2AX as a genomic caretaker and p53 as a gatekeeper cooperate to protect against tumorigenesis.

40. Brown KD, Rathi A, Kamath R, Beardsley DI, Zhan Q, Mannino JL, Baskaran R: **The mismatch repair system is required for S-phase checkpoint activation**. *Nat Genet* 2003, **33**:80-84.

41. Franchitto A, Pichierri P, Piergentili R, Crescenzi M, Bignami M, Palitti F: **The mammalian mismatch repair protein MSH2 is required for correct MRE11 and RAD51 relocalization and for efficient cell cycle arrest induced by ionizing radiation in G2 phase**. *Oncogene* 2003, **22**:2110-2120.

Absence of Procarboxypeptidase R Induces Complement-Mediated Lethal Inflammation in Lipopolysaccharide-Primed Mice[1]

Suzuka Asai,* Tomoo Sato,*§ Toyohiro Tada,† Tomomi Miyamoto,‡ Noriaki Kimbara,* Noboru Motoyama,¶ Hidechika Okada,*§ and Noriko Okada[2]*

Carboxypeptidase R (CPR) is a heat-labile enzyme found in serum in addition to stable carboxypeptidase N. CPR cleaves the C-terminal basic amino acids, arginine and lysine, from inflammatory peptides such as complement C3a and C5a, bradykinin, and enkephalin. This enzyme is generated from procarboxypeptidase R (proCPR), also known as thrombin-activatable fibrinolysis inhibitor, following cleavage by proteolytic enzymes such as thrombin, plasmin, and trypsin. We generated proCPR-deficient mice by knocking out exons 4 and 5 of the proCPR gene, which are regarded as essential for CPR function. At LPS challenge, there was virtually no difference in lethality among proCPR$^{+/+}$, proCPR$^{+/-}$, and proCPR$^{-/-}$ mice. However, challenge with cobra venom factor, which can activate and deplete almost all complement in vivo, induced a lethal effect on proCPR$^{-/-}$ mice following LPS sensitization which up-regulates C5a receptor expression. In contrast, proCPR$^{+/+}$ and proCPR$^{+/-}$ mice were able to tolerate the cobra venom factor challenge with the limited dose (30 U). Although carboxypeptidase N plays a role in inactivation of inflammatory peptides in vivo, CPR may also be important in the regulation of hyperinflammation. *The Journal of Immunology,* **2004, 173: 4669–4674.**

During inflammation, the levels of complement activation products C3a and C5a increase in plasma (1–5). C3a and C5a not only have potent anaphylactic effects, but they can also cause cell chemotaxis, adhesion, and aggregation via receptors on leukocytes or platelets, which release other inflammatory mediators. Basic carboxypeptidases (CPs)[3] are present in plasma and cleave C-terminal arginine and lysine residues from various peptides including inflammatory mediators (6–9). Carboxypeptidase N (CPN) is present in an active form, whereas carboxypeptidase R (CPR), also known as plasma carboxypeptidase B (CPB), carboxypeptidase U (CPU), or activated thrombin-activatable fibrinolysis inhibitor, exists in a precursor form (procarboxypeptidase R (proCPR)). CPR is generated from its zymogene (proCPR) by thrombin (10), thrombin/thrombomodulin complex (11), or plasmin (10) during coagulation or in response to inflammation (12, 13). Recently, it was demonstrated that CPR inactivated C5a octapeptide more rapidly than did CPN (14), and another study showed that elastase, an enzyme secreted from neutrophils, could convert proCPR to CPR (15). Elastase released from neutrophils accumulates at the site of infection, and might play a role in suppression of inflammation by generating CPR, which inactivates inflammatory peptides such as C5a and bradykinin. In vivo studies showed that in response to inflammation induced by injection of LPS in mice and rats, the mRNA level of proCPR but not that of CPN increased significantly (12, 13). Furthermore, the administration of a lethal dose of LPS to rats exhausted CPR activity in serum (12). These studies suggested that CPR may have an important role in preventing hyperinflammation induced by C5a or other inflammatory peptides. To obtain more in vivo evidence of this CPR function, we generated proCPR-deficient mice to evaluate the role of CPR in regulation of the inflammatory response.

Materials and Methods

Construction of the proCPR gene-targeting vector

The mouse proCPR gene was isolated by screening a mouse 129/SV λFIX II genomic library with mouse proCPR cDNA as a probe. A 23.2-kb *Not*I DNA fragment containing exons 3A-7 was subcloned into pBluescript II SK (−) vector (Stratagene, La Jolla, CA). A 4.3-kb *Eco*RV-*Sal*I proCPR DNA fragment containing exon 6 from the above plasmid was subcloned into a pLoxNeoB-P1/R vector, which is composed of a phosphoglycerate kinase (PKG) promoter, a neomycin (neo) resistant gene, and a PGK poly(A) sequence. The resulting plasmid was used as a positive control for PCR detection of the wild-type allele. A 3.0-kb *Bam*HI DNA region of the above 4.3-kb *Eco*RV-*Sal*I fragment was removed from the plasmid. A 5.0-kb *Eco*RI proCPR DNA fragment containing exon 3B was inserted at the 3′ end of the neo cassette. As a result, the neo cassette was flanked by 1.3 and 5.0 kb of homologous sequences. The 8.0-kb *Bam*HI-*Xho*I fragment containing the neo cassette and the homologous sequences was subcloned into the *Bam*HI-*Xho*I-restricted pPGKTk *Apa*I/R vector composed of a PGK promoter, an HSV thymidine kinase gene, and a PGK poly(A) sequence. The construction of the targeting vector is shown in Fig. 1.

Generation of proCPR-deficient mice

The *Bam*HI-linearized targeting vector was introduced by electroporation into E14 embryonic stem (ES) cells derived from the murine 129/Ola strain with Gene Pulser (two pulses of 300 V and 125 μF; Bio-Rad, Hercules, CA). Selection was started 24 h later with G418 (0.3 mg/ml) and ganciclovir (2 μM), and cells were subsequently cultured for 7 days. Correctly

*Department of Biodefense, Graduate School of Medical Sciences, †School of Nursing, and ‡Animal Center, Nagoya City University, Nagoya, Japan; §Choju Medical Institute, Fukushimura Hospital, Toyohashi, Japan; and ¶National Institute for Longevity Sciences, Ohbu, Japan

Received for publication January 28, 2004. Accepted for publication July 13, 2004.

The costs of publication of this article were defrayed in part by the payment of page charges. This article must therefore be hereby marked *advertisement* in accordance with 18 U.S.C. Section 1734 solely to indicate this fact.

[1] This work was supported in part by a grant for Research on Specific Diseases of the Ministry of Health, Labour, and Welfare, Japan.

[2] Address correspondence and reprint requests to Dr. Noriko Okada, Department of Biodefense, Graduate School of Medical Sciences, Nagoya City University, Mizuho-cho, Mizuho-ku, Nagoya 467-8601, Japan. E-mail address: drnoriko@med.nagoya-cu.ac.jp

[3] Abbreviations used in this paper: CP, carboxypeptidase; proCPR, procarboxypeptidase R; neo, neomycin; ES, embryonic stem; CVF, cobra venom factor; T-TM, thrombin and thrombomodulin complex; PGK, phosphoglycerate kinase.

0022-1767/04/$02.00

targeted ES clones were identified by PCR with a pair of primers specific to the proCPR gene-flanking sequence of the targeting construct (5′-CCA AAGTAAAACCTCCTCACCAAG-3′) and the pLoxNeoB-P1/R vector (5′-GCTATACGAAGTTATTAGGTCCCTCG-3′), respectively, and were confirmed by Southern blot analysis. Germline chimera were generated by Japan SLC (Hamamatsu, Japan). Chimeric mice were produced by microinjecting ES cells from four different targeted clones into C57BL/6 blastocytes. Male chimeras were mated to BALB/c females and germline transmission of the mutant proCPR gene in all progeny was confirmed by PCR and Southern blot analysis of tail DNA. Germline transmission was obtained from one of four clones injected. Brother-sister mating was conducted to generate homozygous proCPR-deficient mutants. The background of their progeny was 129/Ola, BALB/c, and C57BL/6. The experimental protocol was approved by the Animal Studies Committee of Nagoya City University Graduate School of Medical Sciences.

Analysis of genotypes

Genomic DNA was isolated from mouse tail and used for genotypic PCR analysis. PCR products from the wild-type allele derived from primers exon 5^+ (GCTTTCTGTTTGTGGTTCATAGGCTAC) and SA^- (GAAT GTTCTCCAGCAGGTGAAATCA), and from the mutant allele derived from primers neo/4.3 (368^+) (GCTATACGAAGTTATTAGGTCCCTCG) and neo/4.3 (1775^-) (CCAAAGTAAAACCTCCTCACCAAG), were both 1.4 kb. The DNA fragment was amplified with *rTaq* DNA polymerase (Toyobo, Osaka, Japan) for 32 cycles of 94°C for 1 min, 60°C for 90 s, and 72°C for 90 s, followed by 72°C for 10 min. PCR products were separated by electrophoresis on 2% agarose gels and visualized by ethidium bromide staining.

RT-PCR

Total RNA was extracted from mouse liver using TRIzol reagent (Invitrogen Life Technologies, Gaithersburg, MD). cDNA was synthesized from total RNA with Superscript II reverse transcriptase (Invitrogen Life Technologies, San Diego, CA) and used as a template for PCR. The following primers were used; exons 2–3, ex2S (CTGCTCTTCCAAGAACCTCCA) and ex3A (ACACTGTCGACATCAGACGC); exons 1–6, ex1S (GCT TCGCCTTTCAGAGTGG) and ex6A (ACGTGTAGTCATAGCCATC CACG); exons 4–5, ex4S (CTGAACAGCATCCTGACA) and ex5A (GCAGGTGAAATCCATTCTCTGGC); exons 6–10, ex6S (GTGGATG GCTATGACTACACGT) and ex10A (TGTATCTCTCAGGCAGC). DNA was amplified with *rTaq* DNA polymerase for 30 cycles of 95°C for 30 s, 50°C for 30 s, and 72°C for 1 min, followed by 72°C for 5 min. PCR products were analyzed by electrophoresis on 2% agarose gels.

Preparation of fresh sera for measurement of CP activity

$ProCPR^{+/+}$, $proCPR^{+/-}$, and $proCPR^{-/-}$ mice, 8–12 wk of age, were anesthetized with pentobarbital and blood was collected by venipuncture of the inferior vena cava. The blood sample was immediately put into a 1.5-ml Eppendorf tube on ice and incubated overnight at 4°C before centrifugation at 3000 rpm for 15 min at 4°C to remove clots. The supernatant was used as the source of serum for determination of CP activity.

Determination of CP activity

CP activity was determined by means of a colorimetric assay using hippuryl-L-arginine (Peptide Institute, Osaka, Japan) as a synthetic substrate (16, 17). In fresh sera, we found CP activity of the CPR generated during coagulation in addition to that of CPN, which is constantly present in the active form in plasma. Total CP activity in sera was determined before or after preincubation at 37°C for 1 h, conditions which inactivate CPR. All sera were diluted 1/10 in 50 mM Tris-HCl buffer (pH 8.0) before using. In fresh sera, an appreciable amount of unactivated proCPR remained. To convert all proCPR to CPR, thrombin and thrombomodulin complexes (T-TM) were added for determination of total proCPR as follows. For determination of both proCPR and CPN activities, sera were diluted 1/10 in 50 mM Tris-HCl (pH 8.0) containing 2 NIH U/ml thrombin (Nihon Pharmaceutical, Tokyo, Japan), 1.4 μg/ml thrombomodulin (a generous gift from A. Kasei, Tokyo, Japan), and 4 mM $CaCl_2$ (each quantity represented the final concentration), and incubated for 20 min at room temperature. Ten microliters of these samples were mixed with 5 μl of 50 mM hippuryl-L-arginine in 50 mM HEPES (pH 8.2) as the substrate solution before incubation for 1 h at room temperature. After the incubation, 100 μM of 0.25 M phosphate buffer (pH 8.3) and 75 μM 3% cyanuric chloride in 1,4 dioxane were added to the mixtures which were then stirred for 20 s on a vortex mixer and centrifuged at 5,000 rpm for 10 min at 4°C. A 100-μl aliquot of the supernatant of each tube was transferred to a 96-well microtiter plate for measurement of absorbance at 405 nm. Each value was compared with a hippuric acid standard curve and the CP activity of each serum sample was then determined as the amount of hippuric acid produced within 1 h.

Histopathology

$ProCPR^{+/+}$ and $proCPR^{-/-}$ mice, 8–12 wk of age, were killed under anesthesia with pentobarbital. Samples of tissues were immediately fixed in 10% phosphate-buffered formalin, then dehydrated in ethanol, cleared in xylene, and embedded in paraffin. The treated tissues were as follows: brain, heart, lungs, liver, kidneys, intestines, stomach, esophagus, spleen, salivary glands, seminal vesicles, testes, thymus, urinary bladder, trachea, adrenal glands, pancreas, and skeletal muscle. Sections were cut at 3-μm thickness and subjected to H&E staining.

Inflammatory model using LPS injection

For the acute inflammatory model, mice were injected i.p. with 15 mg/kg body weight of LPS (*Escherichia coli* O111:B4, Sigma-Aldrich, St. Louis, MO) dissolved in sterile saline. For the chronic inflammatory model, mice were injected i.p. with 3 mg/kg LPS in sterile saline every 24 h for 1 wk (seven times).

Complement activation model using cobra venom factor (CVF)

CVF was purified from lyophilized cobra venom (*Naja naja*; Sigma-Aldrich) as described elsewhere (16). Each mouse was injected i.p. with 100 U of CVF or injected i.v. into the tail vein with 200 U of CVF.

Complement activation model using C5aR up-regulation

For up-regulation of C5aR, 5 mg/kg LPS in sterile saline were injected i.v. into the tail (18). After 6 h, CVF was injected i.p. at a dose of 30 U/mouse. As a control group, some mice were not injected with CVF.

Guinea pig skin test for anaphylatoxin activity

The mouse serum was incubated with 1 mg/ml zymosan A (Sigma-Aldrich) at 37°C for 1 h and centrifuged at 1000 rpm for 5 min to remove this agent. As a control, the mouse serum was incubated without zymosan A using the same conditions. Guinea pigs were injected i.v. with 4 mg of Evans blue (Nacalai Tesque, Kyoto, Japan) 30 min before intradermal injection of 50 μl of mouse serum. After 1 h, guinea pigs were killed by stunning and cervical dislocation before removal of the skin. The blue spots were evaluated from the inner surface of the skin.

Results

Analysis of genotypes

Genomic DNA from mouse tails was used for genotyping by PCR. One of the primers used to detect the wild-type allele matched sequences within exon 5 of proCPR and the other matched that within the intron preceeding exon 6 of proCPR. Therefore, the bands synthesized with these primers were detected only with genomic DNA of $proCPR^{+/+}$ and $proCPR^{+/-}$ mice. In contrast, both of the primers for detecting the mutant allele matched the sequences included in the neo vector sequences, and the bands were synthesized with only the genomic DNA of $proCPR^{-/-}$ and $proCPR^{+/-}$ mice (Fig. 1*b*).

RT-PCR with liver mRNA

To confirm the deficiency of proCPR mRNA, RT-PCR was performed with four sets of primers to detect four positions on the mRNA isolated from the liver. All of the PCR products were full length for the mRNA from the $proCPR^{+/+}$ mouse (Fig. 2). In contrast, with the mRNA of the $proCPR^{-/-}$ mouse, the sizes of the PCR product of exons 1–6 were shorter by ~200 bp than those of $proCPR^{+/+}$, although those of exons 2–3 and 6–10 were the same as those of the $proCPR^{+/+}$ mouse. The 200 nucleotide bp length was consistent with the length of exons 4 and 5 coding for proCPR. A band for exons 4–5 was not detected with mRNA isolated from the $proCPR^{-/-}$ mouse. With mRNA from $proCPR^{+/-}$mice, the bands detected on the agarose gel consisted of all the sizes found with both $proCPR^{+/+}$ and $proCPR^{-/-}$ mice. This confirmed generation of the $proCPR^{+/-}$ and $proCPR^{-/-}$ mice. ProCPR synthesized in the $proCPR^{-/-}$ mice is defective in the region encoded by

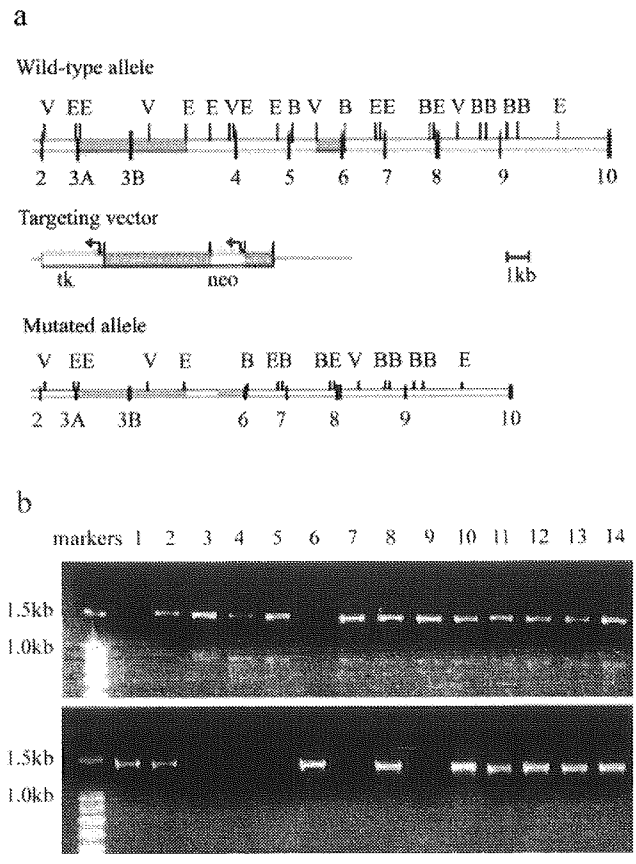

FIGURE 1. *a*, Targeting strategy to disrupt the murine proCPR gene. Restriction maps depict the wild-type allele (*top*), targeting vector (*middle*), and the mutated allele (*bottom*). Exons 4 and 5 encoding some of the zinc and substrate binding sites of proCPR were replaced with a neomycin resistance gene (neo). The shaded region represents the 5′ and 3′ flanks used for homologous recombination. Exons are represented by black boxes. B, E, and V indicate *Bam*HI, *Eco*RI, and *Eco*RV sites. *b*, The genomic DNA isolated from mouse tails were used for genotypic PCR analysis. The PCR products from the wild-type allele are shown in the *upper panel* and those from the mutant allele are shown below. Both bands are ~1400 bp. proCPR$^{+/+}$, proCPR$^{+/-}$, and proCPR$^{-/-}$ mice were nos. 3, 4, 5, 7, and 9, nos. 2, 8, and 10–14, and nos. 1 and 6, respectively.

exons 4 and 5, which includes the genes for two of three zinc-binding sites and one of nine substrate-binding sites in humans (10).

Ratios of the three genotypes among generational offspring

We generated 129/B6/BALB/c (129/Ola, C57BL/6, and BALB/c) proCPR-deficient mice. By the mating of male 129/B6 (129/Ola and C57BL/6) chimeras and female wild-type BALB/c, we obtained one proCPR$^{+/-}$ F_1 mouse. This proCPR$^{+/-}$ mouse was mated with other wild-type littermates, and proCPR$^{+/+}$ and proCPR$^{+/-}$ F_2 offspring with the strain backgrounds of 129/B6/BALB/c were obtained. ProCPR$^{+/+}$, proCPR$^{+/-}$, and proCPR$^{-/-}$ F_3 mice were generated by the mating of proCPR$^{+/-}$ F_2 mice. However, as shown in Table I, proCPR$^{-/-}$ F_3 mice represented only 14 of 124, and proCPR$^{-/-}$ F_4 mice represented 9 of 138. The ratios of these offspring did not conform to Mendel's laws.

CP activity of sera from proCPR-deficient mice

The CP activity of sera from a proCPR$^{-/-}$ mouse and a proCPR$^{+/-}$ mouse was determined and compared with that of a proCPR$^{+/+}$ mouse. Because only a portion of proCPR is activated

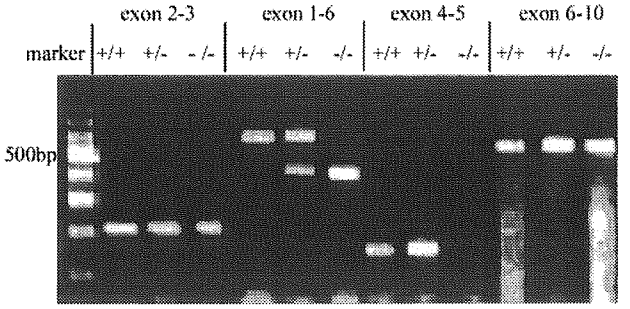

FIGURE 2. RT-PCR analysis of liver mRNA. All of the PCR products were obtained in full length with the mRNA from proCPR$^{+/+}$ and proCPR$^{+/-}$. In contrast, there was no product using mRNA from proCPR$^{-/-}$ lacking exons 4–5. The product obtained with mRNA from proCPR$^{-/-}$ and one of two obtained with that of proCPR$^{+/-}$ corresponding to exons 1–6 were shorter by ~200 bp than that of proCPR$^{+/+}$ (full length). The 200-bp nucleotide length was consistent with the length of exons 4 and 5 coding for proCPR.

to CPR during coagulation, the addition of T-TM and Ca^{2+} can be used to activate the remaining proCPR (17, 19). In this experiment, the serum was incubated with T-TM and Ca^{2+} for 20 min at room temperature and then used to determine the total proCPR and CPN activity. The half-lives of CPR in sera of humans and other animals tested were within 6.3–16 min at 37°C (6, 17, 19). Mouse CPR was also labile at 37°C. Therefore, serum incubated for 1 h at 37°C was used to determine CPN activity, because almost all CPR would have been inactivated during the incubation. The CPR activities of proCPR$^{+/+}$, proCPR$^{+/-}$, and proCPR$^{-/-}$ mice were 12.48 ± 1.73 nmol/h (n = 7), 5.03 ± 0.30 nmol/h (n = 8), and 0.60 ± 0.17 nmol/h (n = 12), respectively, and CPN activities were 4.79 ± 0.35 nmol/h (n = 7), 5.01 ± 0.16 nmol/h (n = 8), and 5.00 ± 0.13 nmol/h (n = 12), respectively (Fig. 3).

Histopathology

Possible morphological abnormality was observed in the kidney. The epithelial cells lining the inner surface of most of the renal Bowman's capsules of the proCPR$^{-/-}$ mouse kidney, many of which were flat in the proCPR$^{+/+}$ mice, showed a cuboidal shape continuing to the proximal urinary tubular cells (Fig. 4). This change was seen only in some renal glomeruli of proCPR$^{+/+}$ mice (n = 5), however, proCPR$^{-/-}$ mice (n = 4) showed a significant increase in the number of changes; the mean (mean ± SD) percentages of glomeruli with this change were 73 ± 7.5% in proCPR$^{-/-}$ mice, and 24 ± 3.5% in proCPR$^{+/+}$ mice. Statistical analysis using the Mann-Whitney U test showed significant difference between the two groups (p = 0.0143).

Inflammatory models induced by LPS injection

In preliminary experiments, a portion of proCPR$^{+/+}$ mice survived the i.p. challenge with 15 mg/kg LPS although none survived challenge with 30 mg/kg LPS. Therefore, we used 15 mg/kg LPS to demonstrate increased susceptibility to LPS in proCPR$^{-/-}$ mice. However, some of the proCPR$^{-/-}$ mice survived the LPS

Table I. *Genotypes of F_3 and F_4 offspring of proCPR$^{+/-}$ mating*

	Genotype	+/+	+/−	−/−
F_3	Number of mice	43	67	14
	Percentage of total (%)	35	54	11
F_4	Number of mice	44	85	9
	Percentage of total (%)	32	62	6

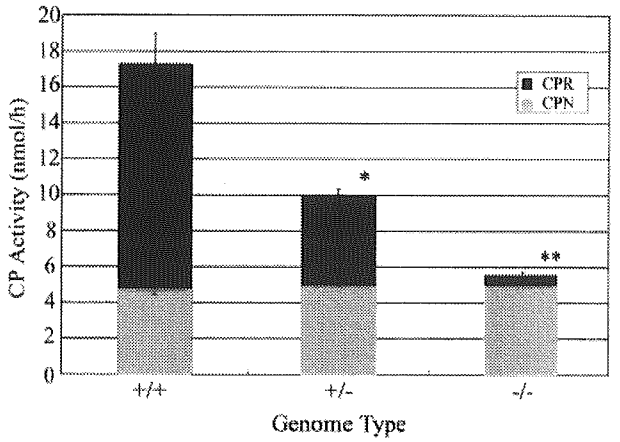

FIGURE 3. CPR activities in all mice groups. Sera were collected from proCPR$^{+/+}$, proCPR$^{+/-}$, and proCPR$^{-/-}$ mice and their CP activities were determined. CPR activities per 1 μl of serum were 12.48 $\pm$1.73 nmol/h, 5.03 $\pm$ 0.30 nmol/h, and 0.60 $\pm$ 0.17 nmol/h, respectively (*, $p < 0.001$, **, $p < 0.0001$; Student's t test), and the CPN activities per 1 μl of sera were 4.79 $\pm$ 0.35 nmol/h, 5.01 $\pm$ 0.16 nmol/h, and 5.00 $\pm$ 0.13 nmol/h, respectively. Each point represents the mean $\pm$ SE (n = 7–12).

challenge as did other types of mice. (Table II). For a chronic inflammation model, a lower concentration of LPS (3 mg/kg) was injected i.p. every 24 h for 1 wk (seven times). After the first injection, some mice in all groups died, and additional deaths occurred from the second to fifth injections (Fig. 5). However, the remaining mice recovered and lived for at least 1 wk after the final LPS injection. From this data, no difference was noted between the proCPR$^{-/-}$ group and any other group of mice.

Complement activation model obtained with CVF following LPS sensitization

As CVF is a strong activator of the alternative complement pathway (20), its injection induces an enhanced production of anaphylatoxins C3a and C5a. Because CVF injection did not result in serious symptoms under normal conditions, we hypothesized that CPR could play an important role in inactivation of these anaphylatoxins in the acute phase. However, i.v. injection of CVF even at a high dose (200 U) did not induce lethal shock in proCPR$^{-/-}$ mice (Table III). It was reported that an i.v. injection of LPS induced the up-regulation of C5aR in mice and rats (18, 21). Furthermore, LPS sensitization of rats induced lethal shock with i.v. injection of a mAb to Crry, a membrane inhibitor of C (22). Therefore, we injected CVF i.p. 6 h after i.v. injection of LPS (5 mg/kg). In preliminary experiments, sensitization of mice with 5 mg/kg LPS rendered the mice, including proCPR$^{+/+}$ mice, susceptible to lethal challenge with 200 U of CVF and proCPR$^{+/-}$ mice susceptible to challenge with 50 U of CVF. Therefore, we used 30 U of CVF to demonstrate the difference in the susceptibility between the proCPR$^{-/-}$ mice and other mice following LPS sensitization (Table III). The survival rate of proCPR$^{+/+}$ and proCPR$^{+/-}$ mice 24 h after the CVF injection was 100% and only one proCPR$^{+/-}$ mouse died 3 days later. In contrast, 6 of 10 proCPR$^{-/-}$ mice died within 24 h of CVF injection.

Inflammatory activity of proCPR$^{-/-}$ mice sera in guinea pig skin

Local inflammation in the skin of guinea pig induced by inoculation of mouse serum was visualized with exudation of Evans blue injected i.v. (Fig. 6). Exudation only occurred where proCPR$^{-/-}$ serum was inoculated, and the lesion was apparently stronger at sites inoculated with proCPR$^{-/-}$ mouse serum treated with zymosan A. However, proCPR$^{+/+}$ serum induced no exudation even after treatment with zymosan A. Repeated experiments gave the same result.

Discussion

The proenzyme of CPR (proCPR) is synthesized in the liver (10, 12, 13) as is the case with that of CPN (23, 24). Human CPR has nine substrate-binding sites and three zinc-binding sites (10), and of these, one substrate-binding and two zinc-binding sites are encoded by the exon 5 region. Therefore, we generated proCPR-deficient mice by knocking out the portion of the gene containing exons 4 and 5. Results of carrying out RT-PCR with total RNA prepared from the liver suggested that proCPR synthesized in the liver of proCPR$^{-/-}$ mice would be an incomplete peptide. CPR activity in sera of proCPR$^{+/-}$ mice was ~30% that of proCPR$^{+/+}$ mice, whereas proCPR$^{-/-}$ mice had little CPR activity at a level which was 3% that of proCPR$^{+/+}$ mice. It remains to be determined whether sera of mice harboring the mutant proCPR gene

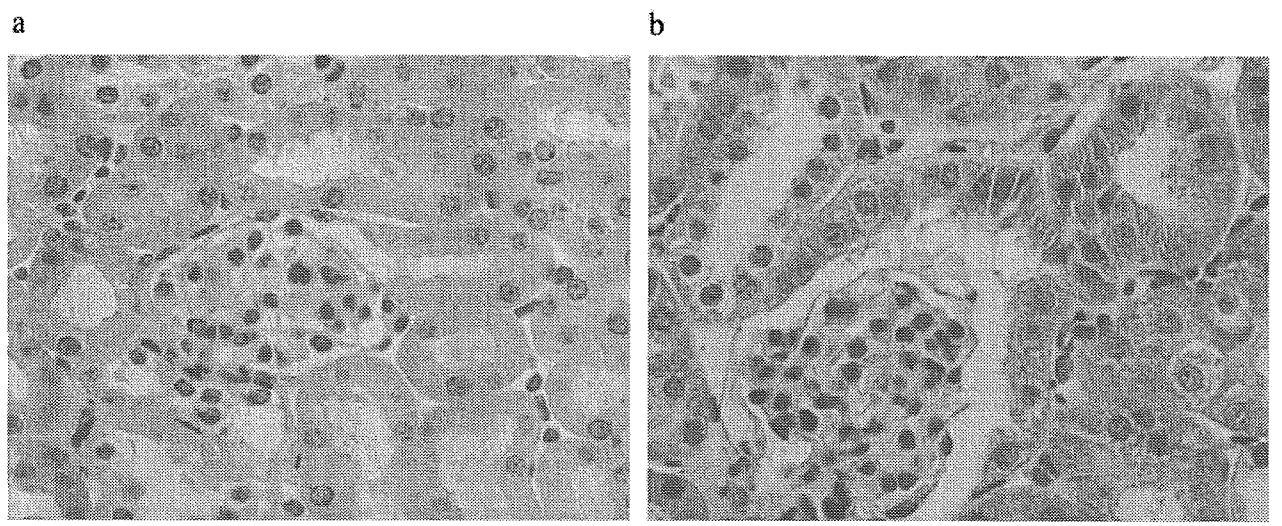

FIGURE 4. Histological features of Bowman's capsule of kidneys of mice. Many cells of Bowman's parietal epithelium of the proCPR$^{+/+}$ mouse are flat in shape (*a*). In contrast, most epithelial cells lining the inner surface of Bowman's capsule of the proCPR$^{-/-}$ mouse are cuboidal extending to the proximal urinary tubular cells (*b*).

Table II. *Effect of LPS on survival rate*

Genotype	Survival	Total	Rate (%)
+/+	6	9	67
+/−	7	10	70
−/−	7	9	78

deficient in exons 4 and 5 could retain a slight amount of CPR activity. Although it was reported that CPN is stable at 37°C for at least 25 min (6, 19), murine CPN activity might have been impaired during the 1-h incubation at 37°C performed to inactivate CPR completely. If this were the case, CPN activity in fresh serum of proCPR$^{-/-}$ mice would be slightly higher than that in serum incubated for 1 h at 37°C.

Thrombin-activatable fibrinolysis inhibitor (proCPR)-deficient mice generated from 129/Sv and C57BL/6 (25) were reported to have delivered the Mendelian ratio with the heterozygote (+/−) intercross. However, although the proCPR-deficient mice produced here developed normally, the genomic ratios of F_3 and F_4 offspring of proCPR$^{+/-}$ intercrosses were not in accordance with Mendel's laws. Disaccordances for F_3 and F_4 offspring were $p < 0.001$ and $p < 0.00001$ using the χ^2 goodness-of-fit test. The proCPR-deficient mice used in this study have a background of 120/Ola, C57BL/6, and BALB/c. Therefore, the BALB/c background might be related to the suppressed number of proCPR$^{-/-}$ offspring. ProCPR might have a role in protecting the fetus in early ontogeny from some stress affecting mice with a BALB/c background.

Some cuboidal transformation of epithelial cells lining Bowman's capsules is normally seen in kidneys of mice (26) and humans (27), but in the present study, the incidence of this was significantly higher as seen from the increased number of affected glomeruli in the proCPR$^{-/-}$ mice compared with the control mice. It could be hypothesized that these cuboidal epithelial cells might aid in some active transport process such as reabsorption of protein (28), but the pathological significance of this change is not well understood. These cuboidal cells were similar to those of proximal convoluted tubules, and might therefore be a metaplasia of Bowman's parietal epithelium (29). In contrast, this epithelial morphology had some resemblance to fetal glomerular structure, and it is possible that a disturbance in histological differentiation was induced in the proCPR$^{-/-}$ mice. Because the mice of 129 background could have certain abnormalities, further analysis is remaining to determine whether the morphological abnormality in the kidney could be a direct consequence of the gene targeting, and whether the morphological abnormality might induce functional disturbance.

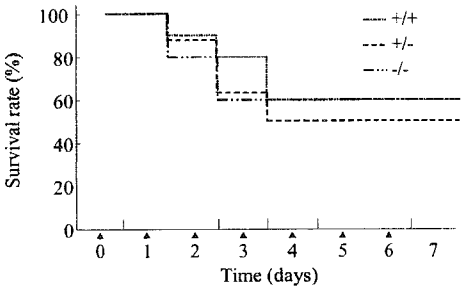

FIGURE 5. Effect of low concentration of LPS. Survival rates of mice were recorded after every injection of LPS (3 mg/kg). LPS dissolved in saline was injected i.p. every 24 h for 1 wk (▲).

Table III. *Effect of CVF injection on survival rate*

	Genotype	Survival	Total	Rate (%)
LPS (5 mg/kg) i.v.	+/+	5	5	100
	+/−			
	−/−	6	6	100
CVF (100 U) i.p.	+/+	3	3	100
	+/−	2	2	100
	−/−	5	5	100
CVF (200 U) i.v.	+/+	12	12	100
	+/−	10	10	100
	−/−	10	10	100
LPS (5 mg/kg) i.v.[a] + CVF (30 U) i.p.	+/+	7[b]	7	100
	+/−	7[b,c]	7	100
	−/−	4[b,d]	10	40

[a] The interval between LPS injection and CVF injection was 6 h.
[b] Difference between proCPR$^{-/-}$ group and other groups is significant ($p < 0.05$; Cochran method).
[c] One mouse died 3 days later.
[d] Six mice died within 24 h.

ProCPR has been established as an acute phase protein (12, 13) because of the up-regulation of mouse proCPR mRNA expression in the liver and proCPR protein in plasma after LPS injection. Therefore, proCPR-deficient mice might be more sensitive to LPS-induced inflammation. When we injected a sublethal dose of LPS into proCPR$^{+/-}$ and proCPR$^{-/-}$ mice, the survival rate was not different from that of proCPR$^{+/+}$ mice. This indicated that LPS could induce cascades of inflammation independent of C5a and other inflammatory peptides which could be inactivated by CPR.

In a rat model, i.v. administration of mAb against Crry, a membrane inhibitor of C, induced lethal shock following LPS sensitization (22), although the mAb alone did not induce this serious outcome (30). This phenomenon might involve the increased expression of C5aR by LPS (18, 21, 31–33). Therefore, we sensitized mice with 5 mg/kg LPS 6 h before i.v. administration of CVF (20), which activates the alternative complement pathway so completely as to exhaust the total amount of complement in vivo. In preliminary experiments, mice sensitized with the LPS preparation hardly survived administration of 200 U of CVF (to proCPR$^{+/+}$ mice) and 100 U of CVF (to proCPR$^{+/-}$ mice), although 50 U of CVF

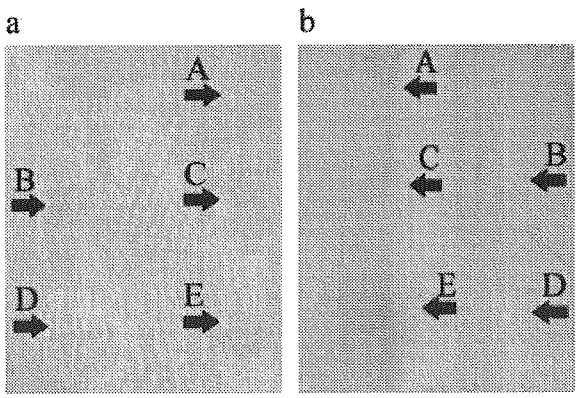

FIGURE 6. *a*, Guinea pig skin observed from the outer surface 1 h after the intradermal injection of 50 μl of mice sera. *b*, Reverse side of the skin. As a control, saline was injected at point A. ProCPR$^{+/+}$ and proCPR$^{-/-}$ sera were injected at points B and C, respectively. ProCPR$^{+/+}$ and proCPR$^{-/-}$ sera which were incubated with zymosan A were injected at points D and E, respectively. Significant Evans blue exudation from vascular sites (blue spots) was observed at E, and faintly at C from the oversurface. No spot was observed at the proCPR$^{+/+}$ serum site even after treatment with zymosan A. Reverse side of the skin showed a strong blue spot at E and was scarcely detected elsewhere even at C.

killed all proCPR$^{-/-}$ mice sensitized with LPS. In mice pretreated with LPS, C5aR had been up-regulated and the extensive generation of C5a could overcome restriction by CPR in proCPR$^{+/+}$ mice. Therefore, we used 30 U of CVF to compare the sensitivity in proCPR$^{+/+}$, proCPR$^{+/-}$, and proCPR$^{-/-}$ mice presensitized with LPS. We found that the injection of 30 U of CVF 6 h after i.v. injection of LPS induced lethality only in proCPR$^{-/-}$ mice but not in proCPR$^{+/+}$ or proCPR$^{+/-}$ mice. This result suggests that CPR generated from proCPR in vivo plays a role in regulation of excessive inflammation due to inflammatory peptides such as C5a anaphylatoxin generated by C activation, which could be inactivated by CPR.

The presence of inflammatory peptides such as C5a in the serum of proCPR$^{-/-}$ mice was demonstrated in the guinea pig skin by means of Evans blue exudation (34), and the exudation was strongly enhanced by preincubation of the serum with zymosan A that has a capacity to activate C. In contrast, exudation was not observed with the serum of proCPR$^{+/+}$ and proCPR$^{+/-}$ mice, even after treatment with zymosan A. This evidence indicates that CPR efficiently inactivates inflammatory peptides such as C5a in serum, and the absence of the enzyme delayed the inactivation although the deficient mouse serum contained CPN. This phenomenon could be explained by the finding that C5a octapeptide was efficiently inactivated by CPR but not by CPN (14).

Acknowledgments

We greatly appreciate Dr. William Campbell and Catherine Campbell for English editing of this manuscript.

References

1. Campbell, W. N., X. Ding, and S. E. Goldblum. 1992. Interleukin-1α and -β augment pulmonary artery transendothelial albumin flux in vitro. *Am. J. Physiol. 263:L128.*
2. Bone, R. C. 1992. Toward an epidemiology and natural history of SIRS (systemic inflammatory response syndrome). *J. Am. Med. Assoc. 268:3452.*
3. Jones, D. K. 1990. Markers for impending adult respiratory distress syndrome. *Respir. Med. 84:89.*
4. Stove, S., T. Welte, T. O. Wagner, A. Kola, A. Klos, W. Bautsch, and J. Kohl. 1996. Circulating complement proteins in patients with sepsis or systemic inflammatory response syndrome. *Clin. Diagn. Lab. Immunol. 3:175.*
5. Goya, T., T. Morisaki, and M. Torisu. 1994. Immunologic assessment of host defense impairment in patients with septic multiple organ failure: relationship between complement activation and changes in neutrophil function. *Surgery 115:145.*
6. Campbell, W., and H. Okada. 1989. An arginine specific carboxypeptidase generated in blood during coagulation or inflammation which is unrelated to carboxypeptidase N or its subunits. *Biochem. Biophys. Res. Commun. 162:933.*
7. Redlitz, A., A. K. Tan, D. L. Eaton, and E. F. Plow. 1995. Plasma carboxypeptidases as regulators of the plasminogen system. *J. Clin. Invest. 96:2534.*
8. Shinohara, T., C. Sakurada, T. Suzuki, O. Takeuchi, W. Campbell, S. Ikeda, N. Okada, and H. Okada. 1994. Pro-carboxypeptidase R cleaves bradykinin following activation. *Int. Arch. Allergy Immunol. 103:400.*
9. Bokisch, V. A., H. J. Muller-Eberhard, and C. G. Cochrane. 1969. Isolation of a fragment (C3a) of the third component of human complement containing anaphylatoxin and chemotactic activity and description of an anaphylatoxin inactivator of human serum. *J. Exp. Med. 129:1109.*
10. Eaton, D. L., B. E. Malloy, S. P. Tsai, W. Henzel, and D. Drayna. 1991. Isolation, molecular cloning, and partial characterization of a novel carboxypeptidase B from human plasma. *J. Biol. Chem. 266:21833.*
11. Bajzar, L., J. Morser, and M. Nesheim. 1996. TAFI, or plasma procarboxypeptidase B, couples the coagulation and fibrinolytic cascades through the thrombin-thrombomodulin complex. *J. Biol. Chem. 271:16603.*
12. Kato, T., H. Akatsu, T. Sato, S. Matsuo, T. Yamamoto, W. Campbell, N. Hotta, N. Okada, and H. Okada. 2000. Molecular cloning and partial characterization of rat procarboxypeptidase R and carboxypeptidase N. *Microbiol. Immunol. 44:719.*
13. Sato, T., T. Miwa, H. Akatsu, N. Matsukawa, K. Obata, N. Okada, W. Campbell, and H. Okada. 2000. Pro-carboxypeptidase R is an acute phase protein in the mouse, whereas carboxypeptidase N is not. *J. Immunol. 165:1053.*
14. Campbell, W. D., E. Lazoura, N. Okada, and H. Okada. 2002. Inactivation of C3a and C5a octapeptides by carboxypeptidase R and carboxypeptidase N. *Microbiol. Immunol. 46:131.*
15. Kawamura, T., N. Okada, and H. Okada. 2002. Elastase from activated human neutrophils activates procarboxypeptidase R. *Microbiol. Immunol. 46:225.*
16. Komura, H., K. Obata, W. Campbell, M. Yumoto, Y. Shimomura, H. Katsuya, N. Okada, and H. Okada. 2002. Effect of anticoagulants in colorimetric assay for basic carboxypeptidases. *Microbiol. Immunol. 46:115.*
17. Schatteman, K. A., F. J. Goossens, S. S. Scharpe, H. M. Neels, and D. F. Hendriks. 1999. Assay of procarboxypeptidase U, a novel determinant of the fibrinolytic cascade, in human plasma. *Clin. Chem. 45:807.*
18. Laudes, I. J., J. C. Chu, M. Huber-Lang, R. F. Guo, N. C. Riedemann, J. V. Sarma, F. Mahdi, H. S. Murphy, C. Speyer, K. T. Lu, et al. 2002. Expression and function of C5a receptor in mouse microvascular endothelial cells. *J. Immunol. 169:5962.*
19. Komura, H., Y. Shimomura, M. Yumoto, H. Katsuya, N. Okada, and H. Okada. 2002. Heat stability of carboxypeptidase R of experimental animals. *Microbiol. Immunol. 46:217.*
20. Lachmann, P. J., L. Halbwachs, A. Gewurz, and H. Gewurs. 1976. Purification of cobra venom factor from phospholipase A contaminant. *Immunology 31:961.*
21. Riedemann, N. C., R. F. Guo, V. J. Sarma, I. J. Laudes, M. Huber-Lang, R. L. Warner, E. A. Albrecht, C. L. Speyer, and P. A. Ward. 2002. Expression and function of the C5a receptor in rat alveolar epithelial cells. *J. Immunol. 168:1919.*
22. Mizuno, M., K. Nishikawa, N. Okada, S. Matsuo, K. Ito, and H. Okada. 1999. Inhibition of a membrane complement regulatory protein by a monoclonal antibody induces acute lethal shock in rats primed with lipopolysaccharide. *J. Immunol. 162:5477.*
23. Oshima, G., J. Kato, and E. G. Erdos. 1975. Plasma carboxypeptidase N, subunits and characteristics. *Arch. Biochem. Biophys. 170:132.*
24. Gebhard, W., M. Schube, and M. Eulitz. 1989. cDNA cloning and complete primary structure of the small, active subunit of human carboxypeptidase N (kininase 1). *Eur. J. Biochem. 178:603.*
25. Nagashima, M., Z. F. Yin, L. Zhao, K. White, Y. Zhu, N. Lasky, M. Halks-Miller, G. J. Broze, Jr., W. P. Fay, and J. Morser. 2002. Thrombin-activatable fibrinolysis inhibitor (TAFI) deficiency is compatible with murine life. *J. Clin. Invest. 109:101.*
26. Ahmadizadeh, M., R. Echt, C. H. Kuo, and J. B. Hook. 1984. Sex and strain differences in mouse kidney: Bowman's capsule morphology and susceptibility to chloroform. *Toxicol. Lett. 20:161.*
27. Haensly, W. E., and J. C. Lee. 1986. Metaplasia of the parietal layer of Bowman's capsule: a histopathological survey of the human kidney. *Histol. Histopathol. 1:363.*
28. Hanker, J. S., J. W. Preece, and E. K. MacRae. 1975. Cytochemical correlate of structural sexual dimorphism in glandular tissue of the mouse. I. Studies of the renal glomerular capsule. *Histochemistry 44:225.*
29. Eshenbrenner, A. B., and E. Miller. 1945. Sex difference in kidney morphology and chloroform necrosis. *Science 102:302.*
30. Matsuo, S., S. Ichida, H. Takizawa, N. Okada, L. Baranyi, A. Iguchi, B. P. Morgan, and H. Okada. 1994. In vivo effects of monoclonal antibodies that functionally inhibit complement regulatory proteins in rats. *J. Exp. Med. 180:1619.*
31. Haviland, D. L., R. L. McCoy, W. T. Whitehead, H. Akama, E. P. Molmenti, A. Brown, J. C. Haviland, W. C. Parks, D. H. Perlmutter, and R. A. Wetsel. 1995. Cellular expression of the C5a anaphylatoxin receptor (C5aR): demonstration of C5aR on nonmyeloid cells of the liver and lung. *J. Immunol. 154:1861.*
32. Akatsu, H., T. Miwa, C. Sakurada, Y. Fukuoka, J. A. Ember, T. Yamamoto, T. E. Hugli, and H. Okada. 1997. cDNA cloning and characterization of rat C5a anaphylatoxin receptor. *Microbiol. Immunol. 41:575.*
33. Fukuoka, Y., J. A. Ember, and T. E. Hugli. 1998. Cloning and characterization of rat C3a receptor: differential expression of rat C3a and C5a receptors by LPS stimulation. *Biochem. Biophys. Res. Commun. 242:663.*
34. Nishikawa, K., S. Matsuo, N. Okada, B. P. Morgan, and H. Okada. 1996. Local inflammation caused by a monoclonal antibody that blocks the function of the rat membrane inhibitor of C3 convertase. *J. Immunol. 156:1182.*

THE JOURNAL OF BIOLOGICAL CHEMISTRY
Vol. 279, No. 33, Issue of August 13, pp. 34741–34749, 2004

Printed in U.S.A.

Abnormal Angiogenesis in *Foxo1* (*Fkhr*)-deficient Mice*

Received for publication, December 28, 2003, and in revised form, May 28, 2004
Published, JBC Papers in Press, June 7, 2004, DOI 10.1074/jbc.M314214200

Tatsuo Furuyama‡§, Kazuko Kitayama‡, Yuri Shimoda¶‖, Minetaro Ogawa¶, Kiyoaki Sone‡, Kiyomi Yoshida-Araki, Hiroshi Hisatsune‡‡, Shin-ichi Nishikawa‡‡§§, Keiko Nakayama¶¶, Keiichi Nakayama¶¶, Kyoji Ikeda**, Noboru Motoyama**, and Nozomu Mori‡**

*From the Departments of ‡Molecular Genetics and **Geriatric Research, National Institute for Longevity Sciences, and the ¶Department of Cell Differentiation, Institute of Molecular Embryology and Genetics, Kumamoto University, Kumamoto 860-0811, Japan, the ¶¶Department of Molecular and Cellular Biology, Medical Institute of Bioregulation, Kyushu University, Kyushu 812-8582, Japan the §§Laboratory for Stem Cell Biology, Center for Developmental Biology, RIKEN 650-0047, Japan, and the ‡‡Department of Molecular Genetics, Graduate School of Medicine, Kyoto University, Kyoto 606-8501, Japan*

Members of the *Foxo* family, *Foxo1* (*Fkhr*), *Foxo3* (*Fkhrl1*), and *Foxo4* (Afx), are mammalian homologs of *daf-16*, which influences life span and energy metabolism in *Caenorhabditis elegans*. Mammalian FOXO proteins also play important roles in cell cycle arrest, apoptosis, stress resistance, and energy metabolism. In this study, we generated *Foxo1*-deficient mice to investigate the physiological role of FOXO1. The *Foxo1*-deficient mice died around embryonic day 11 because of defects in the branchial arches and remarkably impaired vascular development of embryos and yolk sacs. *In vitro* differentiation of embryonic stem cells demonstrated that endothelial cells derived from wild-type and *Foxo1*-deficient embryonic stem cells were able to produce comparable numbers of colonies supported by a layer of OP9 stromal cells. Although the morphology of the endothelial cell colonies was identical in both genotypes in the absence of exogenous vascular endothelial growth factor (VEGF), *Foxo1*-deficient endothelial cells showed a markedly different morphological response compared with wild-type endothelial cells in the presence of exogenous VEGF. These results suggest that *Foxo1* is essential to the ability of endothelial cells to respond properly to a high dose of VEGF, thereby playing a critical role in normal vascular development.

The *Foxo* family is one of the forkhead-type transcription factor families and is unique in that its members are downstream components of the insulin signaling pathway involving phosphatidylinositol 3-kinase/Akt (1). They are also mammalian homologs of the *daf-16* gene in *Caenorhabditis elegans*, which is essential for the extension of life span and dauer formation in *C. elegans*. DAF-16 confers resistance to stress such as heat and UV light, and dauer formation is observed under adverse conditions such as food deprivation (2, 3). Just as in *C. elegans*, in mammals, the *Foxo* family functions to regulate the transcription of genes involved in stress resistance and energy metabolism. Genes regulated by FOXO proteins are grouped into four categories. The first group includes the genes for proteins involved in cell cycle arrest and DNA repair such as p27 and GADD45 (4–7). The second group is made up of genes whose products are related to apoptosis such as FasL and Bim (1, 7). The third group comprises genes for proteins related to resistance to oxidative stress such as manganese-containing superoxide dismutase and catalase (8, 9). The last group is composed of genes whose products are involved in energy metabolism such as glucose-6-phosphatase, phosphoenolpyruvate carboxykinase, and insulin-like growth factor-1-binding protein-1 (10–13). We previously reported that each member of the *Foxo* family (*Foxo1* (*Fkhr*), *Foxo3* (*Fkhrl1*), and *Foxo4* (*Afx*)) show a tissue-specific and developmentally specific expression pattern (14). *Foxo4* mRNA is abundant in skeletal muscle throughout life, whereas *Foxo1* mRNA is abundantly found in adipose tissues. *Foxo3a* mRNA is scant during ontogeny, but becomes abundant after birth (14). Moreover, recent studies showed that FOXO1 plays important roles in the differentiation of adipocytes and in the myotube fusion of myoblasts *in vitro* (15, 16). It is therefore suggested that each member plays a distinct role in a tissue-specific and developmentally specific manner *in vivo*. Indeed, studies using *Foxo1* transgenic mice and heterozygous *Foxo1*-deficient mice showed that FOXO1 is involved in the differentiation of beta-cells in the pancreas and energy metabolism (15, 17).

In this study, we generated *Foxo1*-null mice to address the role of FOXO1 *in vivo*. *Foxo1*-null mice died at around embryonic day (E)[1] 11. We found abnormal angiogenesis in the yolk sacs and embryos as well as underdevelopment of branchial arches at around E9.5. Endothelial cells differentiated from embryonic stem (ES) cells lacking *Foxo1* showed a morphologically abnormal response to exogenous vascular endothelial growth factor (VEGF), *viz.* a flat polygonal morphology in contrast to the elongated spindle-like shape of wild-type endothelial cells. These results suggest that FOXO1 plays a critical role in qualitatively controlling the VEGF signaling pathway and is necessary for normal development of the vascular system early in life.

* The work was supported in part by Grant 12C-05 for longevity sciences from the Ministry of Health, Labor, and Welfare (to T. F.) and the Mochida Memorial Foundation for Medical and Pharmaceutical Research (to M. O.). The costs of publication of this article were defrayed in part by the payment of page charges. This article must therefore be hereby marked "*advertisement*" in accordance with 18 U.S.C. Section 1734 solely to indicate this fact.

§ To whom correspondence should be addressed: Dept. of Food and Nutrition, Sonoda Woman's University, 7-29-1 Minami-Tsukaguchi, Amagasaki, Hyogo 661-8520, Japan. Tel.: 81-6-6429-1201; Fax: 81-6-6422-8523; E-mail: furuyama@sonoda-u.ac.jp.

‖ Supported by the Research for the Future Program of the Japanese Society for the Promotion of Science.

[1] The abbreviations used are: E, embryonic day; ES, embryonic stem; VEGF, vascular endothelial growth factor; mAb, monoclonal antibody; VE-cadherin, vascular endothelial cadherin; RT, reverse transcription; PFA, paraformaldehyde; PBS, phosphate-buffered saline; TBS, Tris-buffered saline; PECAM-1, platelet endothelial cell adhesion molecule-1.

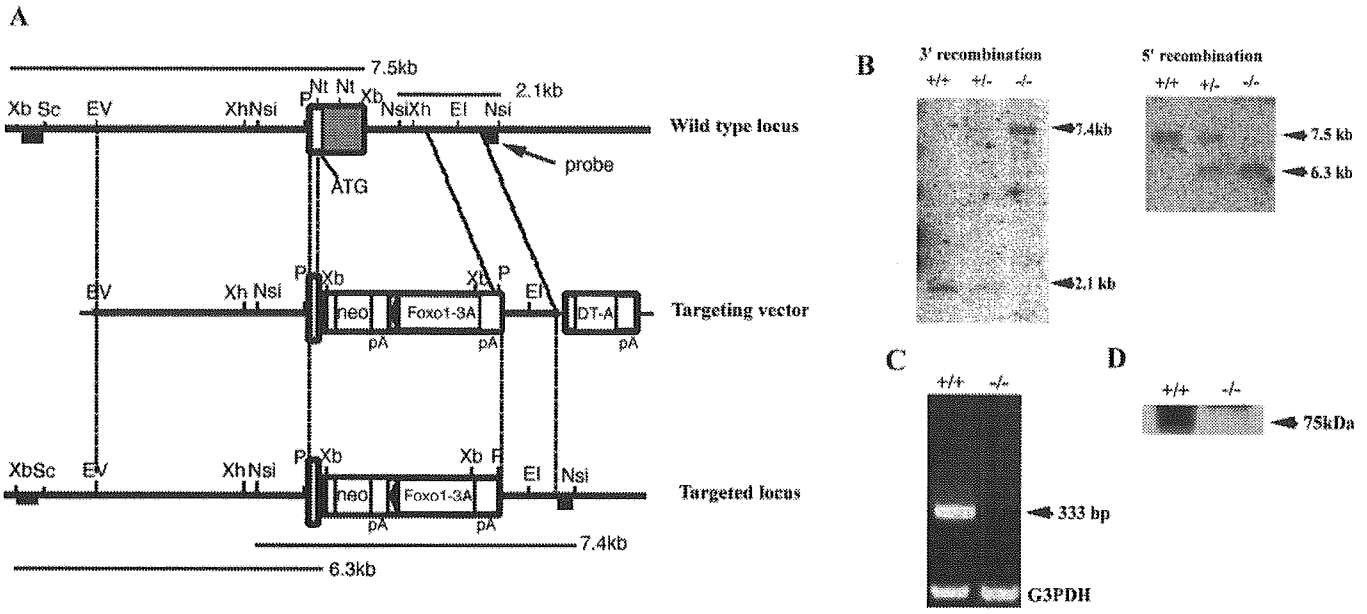

FIG. 1. **Gene targeting of the *Foxo1* locus.** *A*, shown is a schematic of a portion of the *Foxo1* locus with restriction sites, exons (*boxes*), and the resulting targeted locus. Homologous recombination replaced the 5′-noncoding region, and first 208 codons of *Foxo1*, and 1.5 kb of the first intron with a *loxP-PGKneo*-poly(A)-*loxP*-FOXO1-3A-poly(A) cassette. The NsiI restriction fragments confirming the structure of PCR-positive ES clones are indicated. *EI*, EcoRI; *EV*, EcoRV; *Nsi*, NsiI; *Nt*, NotI; *P*, PstI; *Sc*, SacI; *Xh*, XhoI; *Xb*, XbaI; *DT-A*, diphtheria toxin A chain; *pA*, poly(A). *B*, shown are the results from Southern blot analysis of NsiI genomic DNA digests from a wild-type, heterozygous, and homozygous embryo at E9.5. The 3′-probe detected the 2.1- and 7.4-kb restriction fragments corresponding to the wild-type and targeted alleles, respectively. The 5′-probe detected the 7.5- and 6.3-kb restriction fragments corresponding to the wild-type and targeted alleles, respectively. *C*, RT-PCR analysis of total RNA from a wild-type and homozygous embryo at E9.5 detected a specific band only in the wild-type embryo. The primers flanking the ATG codon gave a 333-bp PCR product. *G3PDH*, glyceraldehyde-3-phosphate dehydrogenase. *D*, Western blot analysis of protein from wild-type embryos at E9.5 detected a specific band at ~75 kDa, but no band in homozygous *Foxo1*-deficient embryos.

MATERIALS AND METHODS

Targeted Disruption of the Foxo1 Gene—A 625-bp probe starting from the ATG codon of the mouse *Foxo1* gene was used to screen a 129SVJ genomic library (Stratagene). Analysis of several overlapping clones revealed that the first coding exon including the ATG codon ends 625 bp after the ATG codon. Further phage analysis revealed that the rest of the coding exons are not located within at least 15 kb downstream from the first coding exon. To construct a targeting vector, a 5-kb EcoRV-NotI fragment whose 3′-end terminated 330 bp upstream of the ATG codon was used as the 5′-arm. A 4.2-kb *loxP-PGKneo*-poly(A)-*loxP*-FOXO1-3A-poly(A) cassette, in which FOXO1-3A is a constitutively active form of the FOXO1 protein in terms of transcriptional activity, was used to replace a 2.5-kb sequence including a 1-kb sequence 3′ to the first NotI site in the first exon and a 1.5-kb intronic sequence following the first exon. A downstream 1.1-kb PCR fragment was used as the 3′-arm. Finally, a 1.3-kb cassette containing the diphtheria toxin A chain gene was added to the 3′-end of the 3′-arm to facilitate negative selection. The plasmid was linearized with KpnI and electroporated into ES cells. Cells were selected with G418 (Invitrogen). G418-resistant clones were screened by PCR with primers for the sequence flanking the 1.2-kb short arm to confirm a corrective recombination of the 3′-arm. Normal (2.1 kb) and targeted (7.4 kb) loci were distinguished by NsiI digestion when probed with a 300-bp SacI genomic fragment for 3′-arm recombination (Fig. 1*B*). Normal (7.5 kb) and targeted (6.3 kb) loci were distinguished by XbaI digestion when probed with a 400-bp SacI-XbaI genomic fragment for 5′-arm recombination (Fig. 1*B*). Six correctly targeted ES cell clones were expanded, microinjected into C57BL/6J blastocysts, and transferred to the uteri of pseudopregnant ICR mice. Chimeric animals were backcrossed onto a C57BL/6J background to screen for germ line transmission. Chimeric males from two independent clones passed the mutant allele to offspring, and the animals from two lines showed identical phenotypes. Tail biopsy or yolk sack genomic DNA was amplified by PCR with primers specific for the wild-type allele and the target (wild-type *Foxo1*, 5′-GCAGAGATTAGCCTTCACGGCATG-3′ (upper) and 5′-TCTATGCTACAACTGATGGCATGG-3′ (lower); and targeted allele, 5′-TCTTCACAATGCCGCCTGAAAGGC-3′ (upper) and 5′-TCTATGCTACAACTGATGGCATGG-3′ (lower)).

To confirm the deficiency of FOXO1 protein, Western blot analysis was performed for proteins of whole embryos at E9.5. They were lysed in radioimmune precipitation assay buffer (50 mM Tris-HCl (pH 7.4) containing 1% Nonidet P-40, 0.25% sodium deoxycholate, 0.1% SDS, 150 mM NaCl, 1 mM EDTA, 1 mM phenylmethylsulfonyl fluoride, 1 mg/ml aprotinin, 1 mg/ml leupeptin, 1 mg/ml pepstatin, and 1 mM NaF), and aliquots of the proteins were separated on 7.5% reducing polyacrylamide gels and blotted onto Immobilon-P polyvinylidene difluoride membranes (Millipore Corp.). The blots were analyzed using a specific antibody against FKHR (Upstate Biotechnology, Inc.) and a standard chemiluminescence detection kit (ECL, Amersham Biosciences).

The generation of ES cells homozygous for the targeted allele was performed using higher concentrations of G418 (18). One cell line heterozygous for the targeted allele was cultured in medium supplemented with 1.2, 1.8, 2.4, 3.0, or 3.6 mg/ml G418. Thirty-three colonies were picked up from the plate with 3.6 mg/ml G418 after selection for 11 days and expanded. The genomic DNA was extracted and analyzed by Southern blotting using the probe specific for *Foxo1* described above. Only one was cloned.

In Vitro Differentiation of ES Cells—*In vitro* differentiation of ES cells was induced as described previously (19). In brief, 5×10^4 ES cells were inoculated into a 25-cm^2 culture flask preseeded with OP9 stromal cells and cultured for 5 days in induction medium (α-minimal essential medium supplemented with 10% fetal calf serum and 5×10^{-5} mol/liter 2-mercaptoethanol) in the absence of leukemia inhibitory factor. Cultured cells were dissociated with cell dissociation buffer (Invitrogen) and stained with fluorescein isothiocyanate-labeled anti-CD31 monoclonal antibody (mAb) (Pharmingen) and allophyco-cyanin-conjugated anti-vascular endothelial cadherin (VE-cadherin) mAb (20). CD31$^+$ and VE-cadherin$^+$ endothelial cells were sorted using a FACSVantage cell sorter (BD Biosciences). Then, 1×10^3 sorted endothelial cells/well were inoculated into either 6-well culture plates or 2-well culture slides preseeded with OP9 stromal cells. Cells were cultured for 3 days in induction medium in the presence or absence of exogenous human VEGF-A_{165} (Genzyme) and subjected to immunostaining of endothelial cell colonies.

Reverse Transcription (RT)-PCR—Total RNA was purified from embryos and the yolk sacs of wild-type and *Foxo1*-null embryos at E9.5 ($n = 3$) using TRIzol (Invitrogen). After an RT reaction using SuperScript II (Invitrogen), quantitative PCR analysis of several genes involved in vasculogenesis and angiogenesis was performed using a QuantiTect SYBR Green PCR kit (QIAGEN Inc.); oligonucleotides specific for angiopoietin-1, angiopoietin-2, VEGF, Flt-1, Flk-1, Tie-1, Tie-2, EphB3, EphB4, ephrin-B2, connexin-37, connexin-40, connexin-43, and smooth muscle α-actin (Proligo Japan); and a Light Cycler system

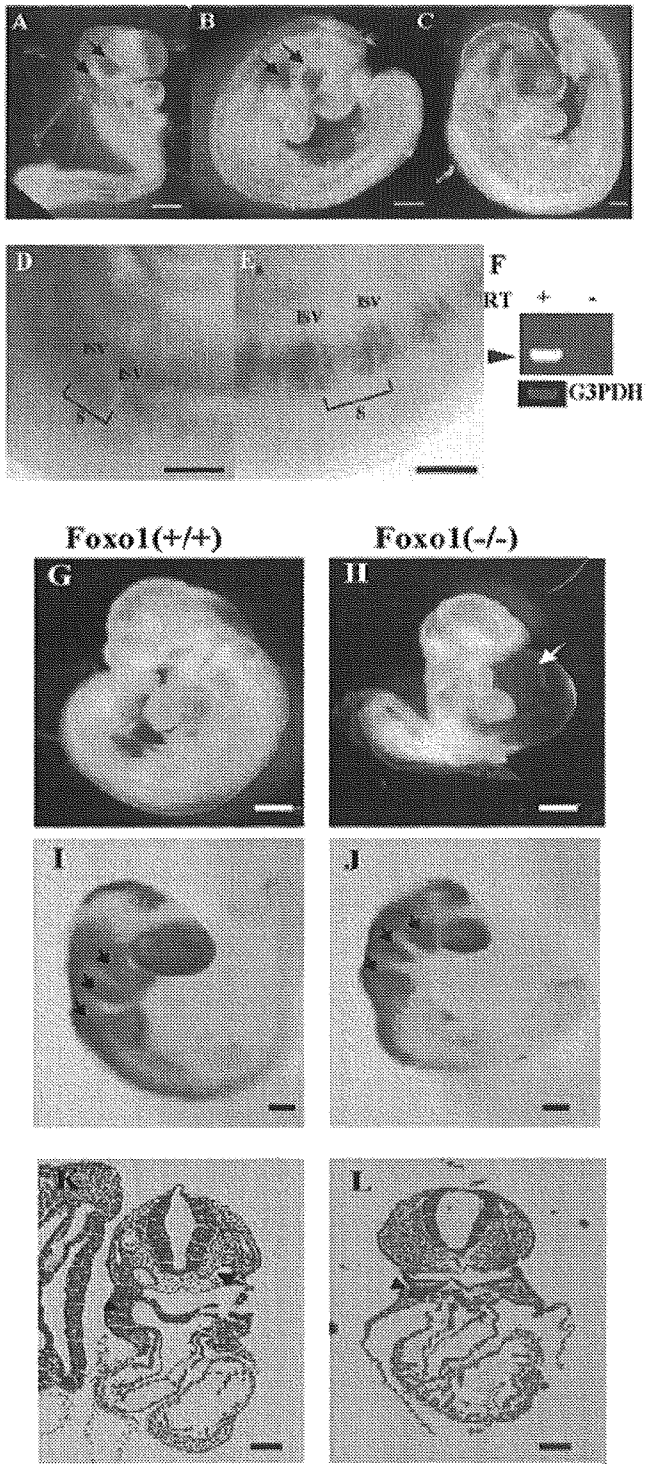

FIG. 2. **Expression of *Foxo1* in embryos and morphological defects in *Foxo1*-deficient mice.** *A*, whole mount *in situ* hybridization revealed *Foxo1* expression in the first branchial arch, migrating neural crest cells in the second branchial arch (*arrows*), and somites of an E8.75 embryo. *B* and *C*, expression localized to the first and second branchial arches (*arrows*) and somites at E9.0 and E9.5, respectively. *D* and *E*, *Foxo1* transcript expression localized in somites (*S*) and intersomitic vessels (*ISV*) at E9.0 and 9.5, respectively. *F*, the expression of *Foxo1* in the yolk sac was below the detection limit of the *in situ* hybridization technique, but RT-PCR confirmed the transcripts to be present in the yolk sac at E9.5. *G3PDH*, glyceraldehyde-3-phosphate dehydrogenase. *G* and *H*, comparison of the appearance of wild-type and *Foxo1*-deficient embryos, respectively, showed apparent growth retardation and a small first branchial arch, but no second branchial arch, and often remarkable pericardial swelling (*arrow*) in E9.5 mutants. *I* and *J*, whole mount *in situ* hybridization with a *Crabp1* antisense probe revealed the pathway of migrating crest cells populating branchial arches at E9.5. Specific staining in wild-type embryos can be seen in streams of cells migrating ventrally into the arches (*arrows*). The staining pattern in the mutant embryos was very similar to that in the wild-type embryos. *K* and *L*, shown is the hematoxylin/eosin staining of transverse sections at the level of the aortic arch. E9.5 *Foxo1*-deficient embryos had dorsal aortas that were severely underdeveloped and irregularly formed in addition to hypoplasia of branchial arches and unclear aortic arch arteries in contrast to wild-type embryos (*arrowheads*). The *arrow* shows the dorsal aorta. *Scale bars* = 200 μm in *A–E*, 300 μm in *G* and *H*, and 150 μm in *I–L*.

(Roche Applied Science). The following conditions were used: 95 °C for 15 min and 25 cycles at 94 °C for 10 s, 58 °C for 20 s, and 72 °C for 20 s. The amount of RT reaction product was controlled on the basis of the expression level of the glyceraldehyde-3-phosphate dehydrogenase housekeeping gene. For confirmation of *Foxo1* mRNA expression, RT-PCR for *Foxo1* was performed using PCR primers specific for *Foxo1* (upper, 5′-ACGAACTCGGAGGCTCCTTAGACAC-3′; and lower, 5′-GACTGGAGGTGGTCGAGTTGGACTG-3′) under the following conditions: 94 °C for 2 min; 35 cycles at 94 °C for 10 s, 63 °C for 30 s, and 72 °C for 45 s; and 72 °C for 2 min. RNA loading was controlled by amplification of the glyceraldehyde-3-phosphate dehydrogenase housekeeping gene. Negative controls were performed for each sample using non-reverse-transcribed RNA.

Histology—For histological analysis, embryos were embedded in paraffin after fixation with 4% paraformaldehyde (PFA). Transverse sections were made at 7-μm intervals throughout the embryos and stained with hematoxylin/eosin solution.

In Situ Hybridization—Whole mount *in situ* hybridization was carried out as described previously (21) with minor modifications. Embryos were collected in ice-cold phosphate-buffered saline (PBS), fixed in 4% PFA in PBS at 4 °C for 3 h, washed with PBS containing 0.1% Triton X-100 (PBST), dehydrated, and stored in methanol at −20 °C until used. After being bleached with 6% hydrogen peroxide in methanol for 2 h at room temperature, embryos were rehydrated though a 75, 50, 25, and 0% methanol and PBST series. Embryos were incubated with 20 μg/ml proteinase K in PBST for 6 min at E8.5~9.0 or for 9 min at E9.5 and refixed in 4% PFA and 0.2% glutaraldehyde in PBS for 20 min. After incubation in hybridization buffer at 63 °C for >4 h, embryos were incubated in the same buffer containing 0.5 μg/ml digoxigenin-labeled RNA probe (Roche Applied Science) at 63 °C for 18 h. The hybridization buffer used and the steps for probe washing, RNase reaction, and RNase inactivation were as described previously (21). After incubation with 10% heat-inactivated goat serum and 2 mM levamisole (Sigma) in Tris-buffered saline (TBS) containing 0.1% Tween 20 (TBST), embryos were treated with 0.24 units/ml anti-digoxigenin Fab fragments (Roche Applied Science) in TBST for 2 h at 4 °C. After a thorough washing with 2 mM levamisole in TBST, embryos were treated with 0.1 M NaCl, 0.1 M Tris-HCl (pH 9.5), 20 mM $MgCl_2$, 0.1% Tween 20, and 2 mM levamisole for 40 min, and hybridization products were visualized using BM Purple (Roche Applied Science) as a substrate. The *Foxo1* and *Crabp1* (cellular retinoic acid-binding protein-1) probe regions used in the *in situ* study were as described previously (14, 22).

Immunochemistry—Whole mount immunohistochemistry was performed with mAb MEC13.3 (rat anti-mouse platelet endothelial cell adhesion molecule-1 (PECAM-1) antibody, Pharmingen) as described previously (23, 24). Embryos were fixed in 2% PFA and PBS at 4 °C for 1 h and dehydrated in methanol. Embryos were bleached in 5% hydrogen peroxide in methanol for 30 min at 4 °C. This was followed by rehydration and blocking in PBS containing 3% skim milk and 0.3% Triton X-100 (PBSMT) at 4 °C twice for 1 h. Embryos were incubated overnight in 10 μg/ml anti-mouse PECAM-1 antibody in PBSMT at 4 °C, washed with PBSMT at 4 °C, and incubated overnight with horseradish peroxidase-conjugated antibody in PBSMT at 4 °C. Embryos were again washed with PBSMT at 4 °C and rinsed in PBST at room temperature for 20 min. For detecting signals, embryos were incubated in 0.3 mg/ml diaminobenzidine (Sigma) in PBST containing 0.5% NiCl for 20 min; hydrogen peroxide was added to a final concentration of 0.015%; and the embryos were incubated for 20–30 min. The staining reaction was terminated by rinsing the embryos in PBST. Embryos were post-fixed overnight in 4% PFA and PBS at 4 °C. To better observe the vasculature, embryos were dehydrated through graded solutions up to 100% methanol.

For the immunochemistry of endothelial cell colonies, 6-well culture plates were fixed in 2% PFA and stained first with purified anti-VE-cadherin mAb (Zymed Laboratories Inc.)and then with horseradish peroxidase-labeled goat anti-rat IgG antibody (BIOSOURCE). VE-cad-

TABLE I
Genotypes of mice resulting from matings of heterozygous FKHR$^{+/-}$ mice

	Genotype		
	FKHR$^{+/+}$	FKHR$^{+/-}$	FKHR$^{-/-}$
9.5 days postcoitus[a]			
Observed	29	39	16
Expected	22	44	22
10.5 days postcoitus[b]			
Observed	6	16	9[c]
Expected	8	16	8
Live births			
Observed	12	17	0
Expected	7	14	7

[a] Genotyping of three embryos in the 9.5-day postcoitus group was inconclusive.
[b] Genotype of one embryo was inconclusive.
[c] Eight of nine FKHR$^{-/-}$ embryos were abnormal and underwent absorption.

herin$^+$ endothelial cell colonies were revealed by the diaminobenzidine/NiCl substrate. For confocal microscopy, 2-well culture slides were fixed in 2% PFA and stained with anti-VE-cadherin mAb. VE-cadherin were immunolocalized by Alexa Fluor 488-labeled goat anti-rat IgG (Molecular Probes, Inc.). Confocal microscopic images of endothelial cell colonies were taken using an Olympus Fluoview laser scanning microscope.

RESULTS

Expression of Foxo1 in Embryos—Whole mount *in situ* hybridization at E8.5 revealed remarkable expression of *Foxo1* in the neural crest cells migrating toward branchial arches and in the putative somites (Fig. 2*A*). The expression of *Foxo1* was subsequently down-regulated and localized to the first and second branchial arches and putative somites at E9.0 and E9.5 (Fig. 2, *B–E*). The expression of *Foxo1* was also observed in the intersomitic vessel, although it could not be determined whether the expression was localized to the endothelial cells (Fig. 2, *D* and *E*). The expression of *Foxo1* in the yolk sac was below the detection limit of the *in situ* hybridization technique. However, RT-PCR confirmed the expression in the yolk sac at E9.5 (Fig. 2*F*).

Targeted Inactivation of the Foxo1 Gene—The replacement vector disrupts the coding sequence by inserting a *loxP-PGK-neo*-poly(A)-*loxP*-FOXO1-3A-poly(A) cassette into the locus (Fig. 1, *A* and *B*). This deletes a portion of the first intron (including the splice donor) and the first 208 codons of the first coding exon, which encodes the N-terminal half of the forkhead domain of FOXO1. Mice heterozygous for the targeted allele were fertile and exhibited no obvious abnormalities. Heterozygous intercrosses yielded no viable offspring that were homozygous for the targeted allele (*Foxo1*$^{-/-}$), consistent with a lethal embryonic phenotype (Table I). The first *Foxo1*$^{-/-}$ embryos were identified at E11.5, having been reabsorbed. Viable embryos were found at E10.5 with beating hearts, but with significant growth retardation. At E9.5, the distribution of *Foxo1*$^{-/-}$ embryos approached the expected mendelian frequencies (Table I). Analysis of embryonic mRNA by RT-PCR revealed *Foxo1* transcripts of the expected length in wild-type embryos, but not in *Foxo1*$^{-/-}$ embryos (Fig. 1*C*). Because an ~75-kDa band of FOXO1 protein detectable in wild-type embryos could not be identified in *Foxo1*$^{-/-}$ embryos by Western blot analyses (Fig. 1*D*), we concluded that no complete form of FOXO1 protein was synthesized in *Foxo1*$^{-/-}$ embryos.

Abnormal Development of Branchial Arches and Aortic Arch Vessels in Foxo1$^{-/-}$ *Embryos*—At E9.0, wild-type and mutant embryos were indistinguishable in size; but after E9.5, *Foxo1*$^{-/-}$ embryos exhibited apparent growth retardation (Fig. 2, *G* and *H*). By E9.5, mutant embryos had developed a small first branchial arch, but no second branchial arch, and often exhibited marked pericardial swelling (Fig. 2, *H* and *J*). Since

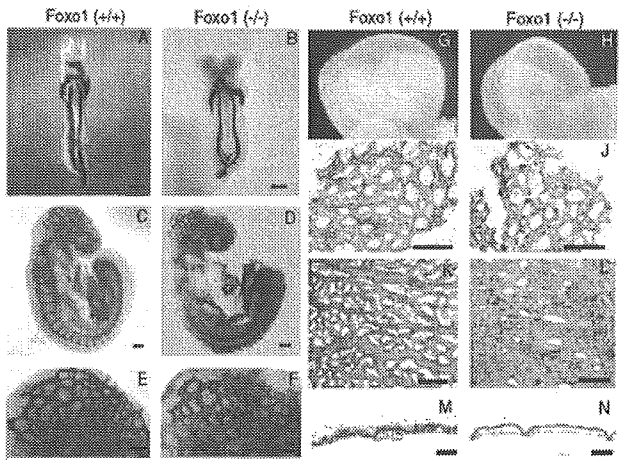

FIG. 3. **Abnormal vascular remodeling in *Foxo1*-deficient embryos.** *A–F* show whole mount immunohistochemical staining of E8.5–9.5 embryos using a mAb against the endothelium-specific marker PECAM-1. Differentiated endothelial cells were observed in wild-type (*A*) and mutant (*B*) embryos at E8.5, and the formation of the dorsal aorta was unaffected by the lack of *Foxo1*. Although the first and second aortic arch arteries were readily apparent in E9.5 wild-type embryos (*C*), there was no evidence of the aortic arch arteries arising from the aortic sacs in mutant embryos (*D*). In the head, the capillary bed appeared dilated in the mutant similar to the yolk sac phenotype (*E*) and apparently arrested at the primary plexus stage (*F*). *G–N* show abnormal vascular remodeling in the yolk sacs of *Foxo1*-deficient embryos. The wild-type yolk sac appeared to have a vasculature (*G*), but the *Foxo1*-deficient yolk sac was pale and had no clear vasculature (*H*). *I–L* show whole mount immunohistochemical staining of E8.75 and E9.5 embryos using a mAb against the endothelium-specific marker PECAM-1. A honeycomb-like vascular plexus was evident by E8.75 (*I*), and subsequent remodeling of the vasculature resulted in defined vessels by E9.5 (*K*). *Foxo1*-deficient yolk sacs showed a honeycomb-like vascular plexus similar to that of wild-type yolk sacs at E8.75 (*J*), but had not developed a normal vasculature at E9.5 (*L*). Histological analysis by hematoxylin/eosin staining revealed that whereas capillary-like vessels containing blood cells with an endothelial cell lining were present in wild-type yolk sacs (*M*), no distinct blood vessels were evident in *Foxo1*-deficient yolk sacs (*N*). *Scale bars* = 160 μm in *A* and *B*, 200 μm in *C–L*, and 50 μm in *M* and *N*.

cranial neural crest cells significantly contribute to the formation of the branchial arches, we followed the pathway of crest cells using whole mount *in situ* hybridization with a *Crabp1* probe as a specific marker for neural crest cells at E9.5. Specific staining in three well defined streams of representing cells migrating ventrally toward the arches could be seen in both wild-type and mutant embryos (Fig. 2, *I* and *J*).

Histological analysis of transverse sections of E9.5 *Foxo1*-deficient embryos revealed that the dorsal aorta was severely underdeveloped and irregularly formed. Hypoplasia of branchial arches and aortic arch arteries was also observed (Fig. 2, *K* and *L*). To examine the extent of vascularization of *Foxo1*-deficient embryos, we performed whole mount immunohistochemical staining at E8.5–9.5 using a mAb against the endothelium-specific marker PECAM-1. We found that the differentiated endothelial cells were present at E8.5 at sites consistent with blood vessel development (Fig. 3*A*) and that the formation of the dorsal aorta was unaffected by the defect in the *Foxo1* gene (Fig. 3*B*). However, there was no evidence of the aortic arch arteries arising from the aortic sacs in the mutant embryos (Fig. 3*D*), whereas the first and second aortic arch arteries were readily apparent in E9.5 wild-type embryos (Fig. 3*C*). The lack of aortic arch vessels most likely resulted in the severe cardiac failure as evidenced by the collection of a large pericardial effusion, with embryonic death occurring soon thereafter. Moreover, the capillary bed appeared dilated and apparently arrested at the primary plexus stage in the heads of

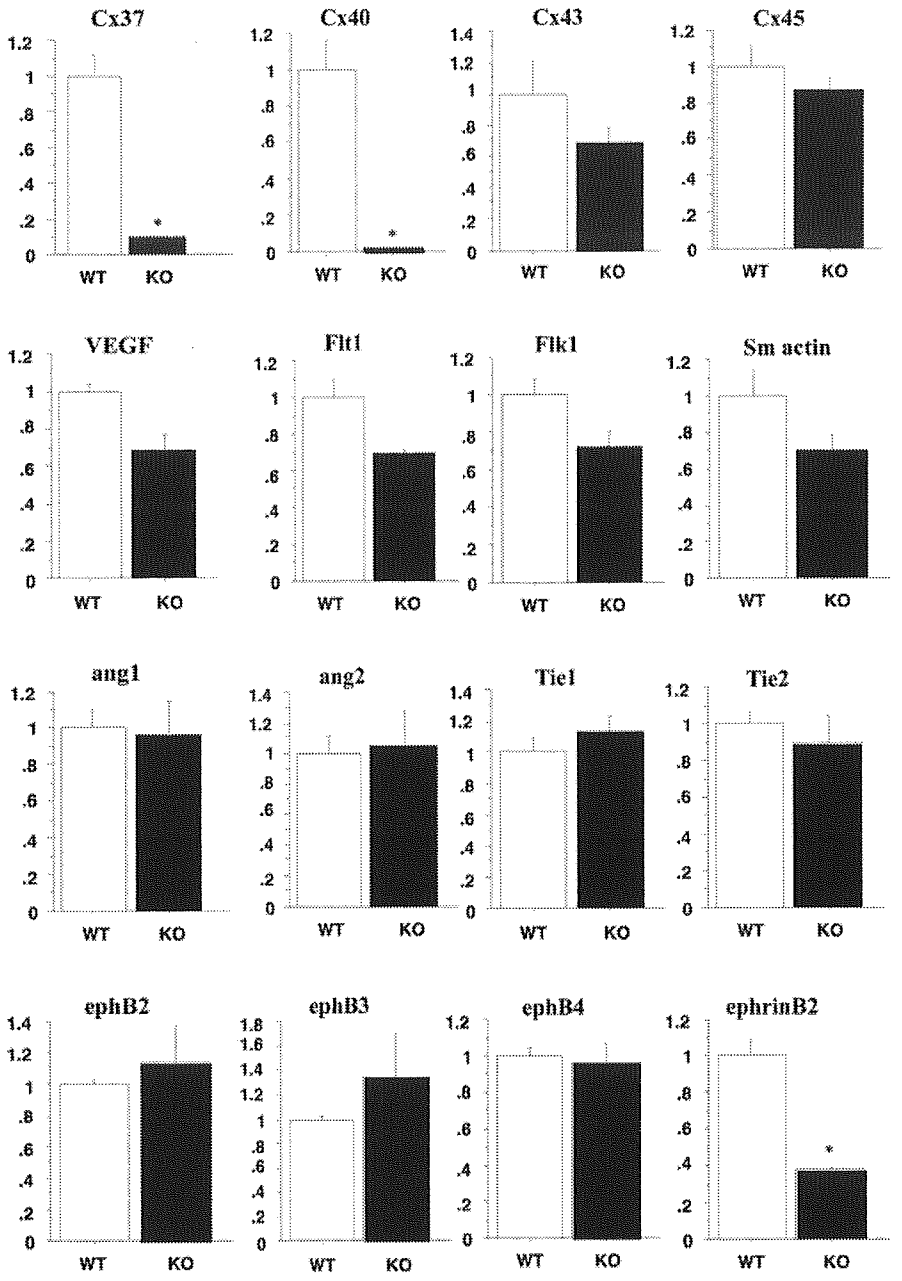

FIG. 4. **Expression of several factors involved in vasculogenesis and angiogenesis.** By quantitative RT-PCR, the expression levels of transcripts for angiopoietin-1 (*ang1*), angiopoietin-2 (*ang2*), VEGF, Flt-1, Flk-1, Tie-1, Tie-2, EphB2, EphB3, EphB4, ephrin-B2, connexin-37 (*Cx37*), connexin-40 (*Cx40*), connexin-43 (*Cx43*), connexin-45 (*Cx45*), and smooth muscle α-actin (*Sm actin*) were examined in the yolk sacs of wild-type (*WT*) and *Foxo1*-deficient (knockout (*KO*)) embryos at E9.5. Data are means ± S.E. of three independent experiments, where the expression level in the yolk sacs of wild-type embryos was regarded as 1.

mutant embryos (Fig. 3, *E* and *F*).

Abnormal Vascular Remodeling in the Yolk Sacs of Foxo1$^{-/-}$ Embryos—The vitelline circulation in the embryonic yolk sac represents the earliest circulatory system and is the first site of vasculogenesis and angiogenesis in the embryo. As shown in Fig. 3 (*G* and *H*), the wild-type yolk sacs appeared to have a vasculature, but the *Foxo1*-deficient yolk sacs were pale and had no clear vasculature. The visceral endoderm and mesoderm forming the yolk sacs were not fused except at discrete foci, giving the yolk sacs of *Foxo1* mutants a characteristic appearance (Fig. 3*H*), with large cavities present in the mutant yolk sacs that were lined by endothelial cells and that contained blood cells. PECAM-1 labeling revealed that endothelial cells were present in both wild-type and *Foxo1*-deficient yolk sacs at E8.75 (Fig. 3, *I* and *J*). Normally, a honeycomb-like vascular plexus was evident by E8.75 (Fig. 3*I*), and subsequent remodeling of the vasculature (angiogenesis) resulted in the formation of large vitelline vessels and a fine network of smaller vessels by E9.5 (Fig. 3*K*). *Foxo1*-deficient yolk sacs showed a honeycomb-like vascular plexus similar to that of wild-type yolk sacs at E8.75 (Fig. 3*J*), but failed to develop a normal vasculature at E9.5 (Fig. 3*L*). Histological analysis revealed that no distinct blood vessels were evident in the *Foxo1*-deficient yolk sacs (Fig. 3*N*), whereas endothelial cell-lined capillary-like vessels containing blood cells were seen in the wild-type yolk sacs (Fig. 3*M*). All together, the above evidence suggests that vasculogenesis (but not angiogenesis) proceeds without functional FOXO1.

To determine whether other molecules contributed to the impaired angiogenesis in the mutants, we examined the expression of several factors and receptors involved in vasculogenesis and angiogenesis. By quantitative RT-PCR analysis, transcripts of VEGF, Flt-1, Flk-1, angiopoietin-1, angiopoietin-2, Tie-1, Tie-2, EphB2, EphB3, EphB4, connexin-43, connexin-45, and smooth muscle α-actin were detected at similar levels, with no statistical significance in wild-type and *Foxo1*$^{-/-}$ yolk sacs at E9.5 (Fig. 4). On the other hand, the expression levels of connexin-37, connexin-40, and ephrin-B2 in

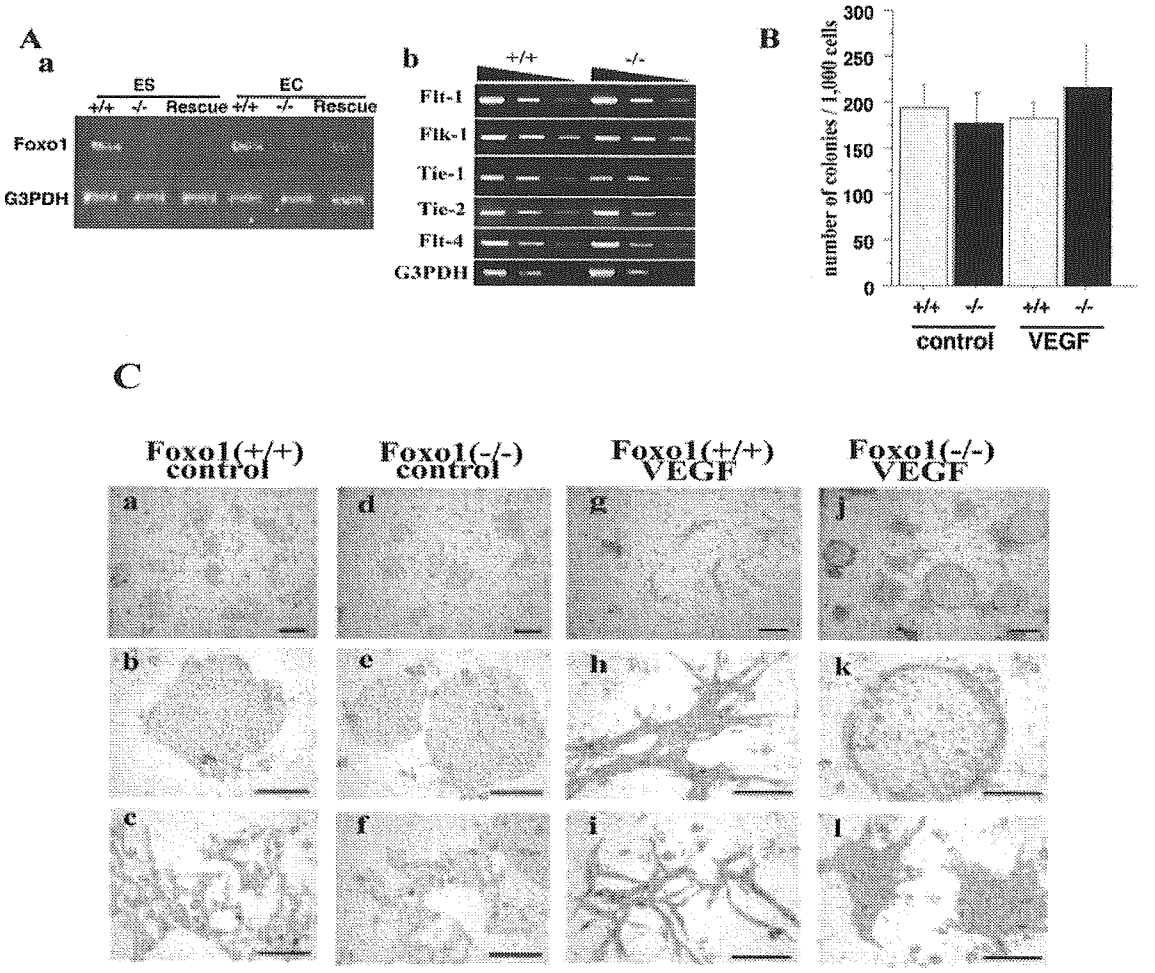

FIG. 5. **Response to exogenous VEGF of endothelial cells derived from *Foxo1*-deficient ES cells cultured on OP9 feeder cells.** *A*: *panel a*, RT-PCR showed that the *Foxo1* transcript was not detected in $Foxo1^{-/-}$ ES cells, the rescued ES cells with VE-cadherin promoter-driven FOXO1, and the endothelial cells (*EC*) from $Foxo1^{-/-}$ ES cells, but was detected in $Foxo1^{+/+}$ ES cells and the endothelial cells from $Foxo1^{+/+}$ and *Foxo1*-rescued ES cells. *G3PDH*, glyceraldehyde-3-phosphate dehydrogenase. *Panel b*, there was no remarkable difference in the expression levels of several genes involved in vascular development between wild-type and *Foxo1*-deficient endothelial cells. *B*: there was no significant difference between the numbers of colonies formed by 1000 $Foxo1^{+/+}$ and $Foxo1^{-/-}$ endothelial cells in the absence or presence of exogenous VEGF-A_{165}. Data are means ± S.E. of four independent experiments. *C*: the morphology of the colonies formed by the endothelial cells of both genotypes was very similar in the absence of exogenous VEGF-A_{165} (*panels a–f*). However, the colonies from *Foxo1*-deficient endothelial cells showed a remarkably different morphology compared wild-type endothelial cells in the presence of 50 ng/ml exogenous VEGF-A_{165} (*panels g–l*). *Scale bars* = 500 μm in *panels a*, *d*, *g*, and *j*, and 200 μm in *panels b*, *c*, *e*, *f*, *h*, *i*, *k*, and *l*.

Foxo1-deficient yolk sacs were significantly reduced to ~10, 1, and 35% of the wild-type levels, respectively ($p < 0.01$). It is possible that the vascular defects in the *Foxo1*-deficient yolk sacs are due in part to the reduction of expression of the specific connexins and ephrin among the molecules examined. However, we cannot eliminate the possibility of changes in unidentified gene expression in specific regions of mutant embryos.

Expression of Foxo1 Transcripts in Endothelial Cells Derived from ES Cells—We demonstrated the presence of *Foxo1* transcripts in the yolk sac (Fig. 2*F*), although the localization could not be determined by *in situ* hybridization. We examined the expression of the *Foxo1* gene in the endothelial cell lineage using an *in vitro* differentiation system composed of ES cells. $Foxo1^{+/+}$ and $Foxo1^{-/-}$ ES cells were co-cultured with OP9 stromal cells to induce differentiation of endothelial cells. Under the culture conditions used in this study, the frequency of endothelial cells among the differentiating ES cells was almost comparable between cultures initiated from $Foxo1^{+/+}$ and $Foxo1^{-/-}$ ES cells (data not shown). $CD31^+$ and VE-$cadherin^+$ endothelial cells were purified using a fluorescence-activated cell sorter and subjected to RT-PCR analysis for the expression of several genes. *Foxo1* transcripts were detected in the endothelial cells derived from $Foxo1^{+/+}$ (but not $Foxo1^{-/-}$) ES cells (Fig. 5*A*, *panel a*), suggesting that *Foxo1* has some functional role in the endothelial cell lineage. Consistent with the observations in the yolk sac described above, transcripts of Flt-1, Flk-1, Flt-4, Tie-1, and Tie-2 were detected at similar levels in $Foxo1^{+/+}$ and $Foxo1^{-/-}$ endothelial cells (Fig. 5*A*, *panel b*), indicating that the expression of these molecules does not depend upon *Foxo1*.

Abnormal Behavior of $Foxo1^{-/-}$ Endothelial Cells in Response to VEGF—Endothelial cells derived from $Foxo1^{+/+}$ and $Foxo1^{-/-}$ ES cells by co-cultivation with OP9 stromal cells were purified using a fluorescence-activated cell sorter and re-cultured on OP9 stromal cell layers to allow colonies to form. The colony formation analysis of endothelial cells derived from ES cells has proved a useful means of revealing the behavior of developing endothelial cells in response to various angiogenic stimuli (19, 25). We took advantage of this culture system to determine whether *Foxo1* has any functional role in endothelial cells. Endothelial cells of the two genotypes gave rise to comparable numbers of colonies (Fig. 5*B*). The addition of 50 ng/ml VEGF-A_{165} to the cultures did not influence the number of colonies formed. Therefore, the results suggest that a lack of